HHS Public Access

Author manuscript

FASEB J. Author manuscript; available in PMC 2021 December 02.

Published in final edited form as:

FASEB J. 2020 August ; 34(8): 10699–10719. doi:10.1096/fj.202000013RR.

Hypochlorhydria reduces mortality in heart failure caused by *Kcne2* gene deletion

Ulrike Lisewski[1], **Clemens Köhncke**[1,2], **Leonhard Schleussner**[1], **Bettina Purfürst**[3], **Soo Min Lee**[4], **Angele De Silva**[4], **Rían W. Manville**[4], **Geoffrey W. Abbott**[4], **Torsten K. Roepke**[1,5]

[1]Experimental and Clinical Research Center, Berlin, Germany

[2]Department of Cardiology, Campus Virchow – Universitätsmedizin Berlin, Berlin, Germany

[3]Electron Microscopy Core Facility, Max-Delbrück-Center for Molecular Medicine, Berlin, Germany

[4]Bioelectricity Laboratory, Department of Physiology and Biophysics, School of Medicine, University of California, Irvine, CA, USA

[5]Department of Cardiology and Angiology, Campus Mitte, Charité – Universitätsmedizin Berlin, Berlin, Germany

Abstract

Heart failure (HF) is an increasing global health crisis, affecting 40 million people and causing 50% mortality within 5 years of diagnosis. A fuller understanding of the genetic and environmental factors underlying HF, and novel therapeutic approaches to address it, are urgently warranted. Here, we discovered that cardiac-specific germline deletion in mice of potassium channel β subunit-encoding *Kcne2* (*Kcne2*$^{CS-/-}$) causes dilated cardiomyopathy and terminal HF (median longevity, 28 weeks). Mice with global *Kcne2* deletion (*Kcne2*$^{Glo-/-}$) exhibit multiple HF risk factors, yet, paradoxically survived over twice as long as *Kcne2*$^{CS-/-}$ mice. Global *Kcne2* deletion, which inhibits gastric acid secretion, reduced the relative abundance of species within Bacteroidales, a bacterial order that positively correlates with increased lifetime risk of human cardiovascular disease. Strikingly, the proton-pump inhibitor omeprazole similarly altered the microbiome and delayed terminal HF in *Kcne2*$^{CS-/-}$ mice, increasing survival 10-fold at 44 weeks. Thus, genetic or pharmacologic induction of hypochlorhydria and decreased gut Bacteroidales species are associated with lifespan extension in a novel HF model.

Correspondence Torsten K. Roepke, Clinic for Internal Medicine/Cardiology Klinikum Niederlausitz, Senftenberg, Germany, torsten.roepke@gmx.net, Geoffrey W. Abbott, Department of Physiology and Biophysics, School of Medicine, University of California, Room D337, Med Sci I, Irvine, CA 92697, USA, abbottg@uci.edu.

AUTHOR CONTRIBUTIONS

U. Lisewski, C. Köhncke, G.W. Abbott, and T.K. Roepke designed research; U. Lisewski, C. Köhncke, L. Schleussner, B. Purfürst, S.M. Lee, and A. De Silva performed research; U. Lisewski, C. Köhncke, L. Schleussner, B. Purfürst, S.M. Lee, A. De Silva, R.W. Manville, G.W. Abbott, and T.K. Roepke analyzed data; U. Lisewski, C. Köhncke, R.W. Manville, G.W. Abbott, and T.K. Roepke generated figures; U. Lisewski, G.W. Abbott, and T.K. Roepke wrote the paper.

Present address

Torsten K. Roepke, Clinic for Internal Medicine/Cardiology Klinikum Niederlausitz, Senftenberg, Germany

DISCLOSURE

Nothing to disclose.

SUPPORTING INFORMATION

Additional supporting information may be found online in the Supporting Information section.

Keywords

dilated cardiomyopathy; heart failure; KCNE; microbiome; potassium channel

1 | INTRODUCTION

Heart failure (HF) is a devastating and increasingly common condition, affecting almost 40 million people worldwide and exhibiting a 50% mortality rate within 5 years of diagnosis.[1,2] The chronic effects of HF involve cardiac muscle weakening to the extent that it can no longer efficiently pump sufficient blood into the aorta, causing pooling of blood in the heart. Coronary artery disease is the most common cause of HF; additional causes include hypertension, dysfunctioning heart valves, cardiomyopathy, myocarditis, and cardiac arrhythmias. The risk of HF increases with metabolic syndrome facets including diabetes and obesity, other chronic diseases including hyper- or hypothyroidism, and lifestyle factors such as inadequate exercise and excessive consumption of sodium- and cholesterol-rich food.[3–5]

Sequence variants in genes encoding ion channel pore-forming (α) subunits, or the proteins that regulate them, are more commonly associated not with HF, but with sudden cardiac death (SCD). Sequence variants in three human genes (*KCNQ1, KCNH2, and SCN5A*) encoding ion channel α subunits account for the large majority of sequenced cases of Long QT syndrome (LQTS), a body-surface electrocardiogram (ECG) anomaly indicative of delayed ventricular repolarization, which underlies many cases of inherited SCD. These causalities are well supported by genetic linkage analyses in large pedigrees.[6–8] Many of the remaining, rarer forms of inherited LQTS associate with ion channel regulatory proteins and each accounts for <1% of sequenced cases. For some, disease association is disputed and not supported by strong linkage analysis,[9–11] for reasons including incomplete penetrance, environmental influences, promiscuity of function, and multiple extracardiac roles. Disease etiology can, therefore, be complex, and disease progression may involve structural heart disease or other extracardiac defects that could exclude the individual harboring the mutation from patient cohorts in studies focusing on “pure” electrical disturbances.

KCNE2 is a prime example, encompassing all four factors. KCNE2 is a single transmembrane domain ancillary (β) subunit that forms complexes with voltage-gated potassium (Kv) channel α subunits, altering channel properties such as voltage-dependence, conductance, gating, trafficking, and pharmacology, thereby generating K^+ currents with properties functionally distinct from those of homomeric Kv channels.[12,13] Inherited variants in KCNE2 are putatively associated with <1% of LQTS cases, but often do not prolong baseline QTc. Instead, they exhibit incomplete penetrance and/or predispose to acquired LQTS only when the individual is challenged with a known QT-prolonging agent such as hERG-blocking drugs including macrolide antibiotics, or electrolyte imbalance.[10,14,15] KCNE2 is a promiscuous β subunit, regulating KCNQ1, hERG, α subunits from the Kv1, 2, 3, and 4 subfamilies,[10,16–23] and even HCN (pacemaker) channels[24] and L-type Ca^{2+} channels.[25] Finally, KCNE2 is widely expressed not only in

cardiac myocytes in both the atria and ventricles, but also in multiple, extracardiac, excitable and non-excitable cell types.[12,26,27]

Consequently, rare human *KCNE2* sequence variants, and more common polymorphisms, associate not only with predisposition to acquired LQTS and in select cases possibly baseline prolonged QTc,[10,14,15] but also with coronary artery disease and/or myocardial infarction.[28–31] Global *Kcne2* germline deletion in mice causes a spectrum of defects—many of which arise from perturbation of its role regulating KCNQ1 in multiple epithelia—including hypothyroidism (and related structural heart disease),[32] achlorhydria,[33,34] type II diabetes mellitus,[35] hypercholesterolemia, hyperkalemia, anemia, elevated angiotensin II,[36] hyperhomocysteinemia, fatty liver,[37] and increased seizure susceptibility.[38] Global *Kcne2* knockout ($Kcne2^{Glo-/-}$) mice also exhibit impaired ventricular myocyte Kv currents, predisposition to acquired LQTS and atherosclerosis—reflecting known human KCNE2 disease correlations—and western diet-induced SCD associated with atrioventricular (AV) block.[23,39,40]

This constellation of defects may reflect potential disease states associated with human *KCNE2* sequence variants, but there are so many interacting lesions in $Kcne2^{Glo-/-}$ mice that the mechanisms underlying the cardiovascular elements are difficult to fully elucidate. Here, we developed and studied mice with cardiac-specific germline *Kcne2* deletion ($Kcne2^{CS-/-}$ mice) to differentiate, for the first time, between intrinsic myocardial effects vs extracardiac effects. This led us to the discovery of an unexpected, early-onset dilated cardiomyopathy phenotype culminating in terminal HF, exhibiting multisystem interactions that suggest hypochlorhydria and associated changes in the gut microbiome as a novel and much-warranted potential therapeutic avenue for delaying terminal HF.

2 | MATERIALS AND METHODS

2.1 | Animals

All experiments involving mice were carried out according to institutional and NIH guidelines. The mice were housed and used according to the recommendations in the Guide for the Care and Use of Laboratory Animals of the National Institutes of Health (NIH Publication, 8th edition, 2011) and were approved by local authorities (LaGeSo Berlin and Institutional Animal care and Use Committee, University of California, Irvine). Global $Kcne2^{-/-}$ mice were generated as previously described[33] and males studied up to 15 months of age. In addition, homozygous mice from a *Kcne2* floxed mouse line (referred to herein as $Kcne2^{lox/lox}$) generated by EUCOMM (The European Conditional Mouse Mutagenesis Program, #41928) were bred with a mouse line expressing Cre-recombinase under the control of the αMHC (alpha myosin heavy chain) promoter[40] to generate a cardiac-specific *Kcne2* knockout strain ($Kcne2^{CS-/-}$), which we first briefly described when we used it as a negative control mouse line for a liver study.[37] Exon 2 of *Kcne2* in $Kcne2^{lox/lox}$ mice is flanked by loxP sites, and therefore, the expression of Cre results in recombination with deletion of exon 2 and inactivation of *Kcne2* by frameshift. Mice were backcrossed into a C57Bl/6 strain background and were maintained in individually ventilated cages under standardized conditions with an artificial 12-hour light-dark cycle, with free access to standard chow (0.25% sodium; SSNIFF Spezialitäten, Soest, Germany) and drinking water

ad libitum. We studied the *Kcne2*$^{CS-/-}$ colony mice at ages up to 8 months. Omeprazole (Sigma Aldrich, St. Louis, MO) was administered via drinking water to give a mean daily dose of 20 mg/kg bodyweight based on expected consumption of 5 mL water per mouse per day. Omeprazole was suspended in a solution of 0.5% (w/v) methylcellulose and 0.2% (w/v) $NaHCO_3$ (pH 9.0) before addition to drinking water. Gastrointestinal hormones were quantified using standard assays by a commercial testing service (Labor 28, Berlin, Germany).

2.2 | Transthoracic echocardiography

For echocardiography we used the Vevo 2010 system (VisualSonics Inc, Toronto, ON, Canada) with a 45-MHz transducer mounted on an integrated rail system. Standard imaging planes, M-mode, and functional calculations were obtained as described before.[23] The LV parasternal short axis view was used to derive fractional shortening (FS), ejection fraction (EF), and ventricular dimensions and volumes as indicated.

2.3 | Electrocardiographic recording and analysis

Electrocardiographic (ECG) monitoring was performed in conscious, restrained mice during the daytime using the EasyCG tools system (EMKA Technologies, Paris, France), as described previously.[41] The system consists of a four-sensor ecgTUNNEL system platform, connected to a wireless transmitter and amplifier system (EMKAPACK). For each individual mouse, continuous ECG registration was performed for 1 hour. For analysis we used the ecg-AUTO software, version 3.3.0.12 (EMKA Technologies, Paris, France). Measurement of standard ECG time-interval parameters was performed on averaged ECG lead II waveforms. The QT interval was corrected for heart rate using Bazett's formula. ECG recording by telemetry. For continuous ECG recording, ECG radio transmitters (TA10 ETA-F20; Data Sciences International, Inc, Saint Paul, MN, USA) were implanted subcutaneously on the backside of the mice under isoflurane anesthesia (Isofluran, Baxter, Unterschleißheim, Germany). Two leads were fixed in the standard lead II position (right upper and left lower thorax). After surgical procedure, the mice were housed in single cages placed over radio receivers (RPC-1 receiver; DSI, Inc Saint Paul, MN, USA). A light-dark run of 12 hours-12 hours was realized to conserve circadian rhythm and excluded from statistical analysis. ECG was performed 1 week after transmitter implantation. For analysis and arrhythmia detection, we used the Ponemah software v. 5.20 (Data Sciences International, Inc, Saint Paul, MN, USA).

2.4 | Patch clamp experiments

Whole-cell patch-clamp recordings were obtained from cardiomyocytes isolated from the mid-ventricular apex. Procedures of ventricular cardiomyocyte isolation and patch clamp recording of K^+ currents followed our standard protocols, which we previously described.[42] For pharmacological isolation of specific K^+ currents we used Hptx2 (500 nmol/L) (Abcam, Cambridge, UK) and 4-AP (50 μmol/L) (Sigma-Aldrich, Saint Louis, USA). Data were analyzed using pClamp9.1 software (Molecular Devices, Sunnyvale, CA), and statistical analysis (ANOVA) was performed using Prism 5.0 (GraphPad Software, Inc, San Diego, CA, USA) and graphically displayed using Origin 8.6 (MicroCal, Northampton, MA, USA).

Freshly dissociated mice cardiomyocytes were kept in a physiological solution with 1 mmol/L Ca^{2+} and 0.5% bovine serum albumin at room temperature (22°−23°C) and used within 6–8 hours. L-type Ca^{2+} current (I_{CaL}) was recorded using the "whole-cell" variant of the patch-clamp method at room temperature (22 ± 2°C). Electrode resistance was 1.3–1.5 MΩ. K^+ currents were blocked by Cs^+. The composition of the standard extracellular solution was (mmol/L): 117 NaCl, 20 CsCl, 2 $CaCl_2$, 1.8 $MgCl_2$, 10 glucose, 10 Hepes, and pH 7.4. The pipette ("intracellular") solution contained (mmol/L): 130 CsCl, 0.4 Na_2GTP, 5 Na_2ATP, 5 Na_2creatine phosphate, 11 EGTA, 4.7 $CaCl_2$ (free Ca^{2+} 108 nmol/L), 20 Hepes, 2 $MgCl_2$; pH was adjusted to 7.2 with CsOH. The Ca^{2+} current was routinely evoked with a double pulse voltage-clamp protocol: from a holding potential of −80 mV a 50-ms prepulse to −40 mV was applied to inactivate the fast Na^+ current. The prepulse was followed by a 300-ms depolarization step to 0 mV. This double pulse was applied every four seconds. After gigaohm seal formation and rupture of the patch, cells were allowed to stabilize for at least 3 minutes before beginning the recordings. Currents were normalized to membrane capacitance and data are presented as current density in pA/pF. We added isoprenaline directly at the cardiomyocyte surface via a micro-pipette at a concentration of 100 nM.

2.5 | Whole-transcript microarray analysis

After euthanasia, mouse ventricular tissue from 3 to 4-monthold mice was harvested, and then, stored at −80°C. When all samples had been collected, total RNA was collected, reverse-transcribed into cDNA, and then, analyzed by "wholetranscript transcriptomics" using the GeneAtlas microarray system (Affymetrix, Santa Clara, CA, USA) and manufacturer's protocols. Mogene 1.1 ST array strips (Affymetrix) were used for hybridization with newly synthesized sscDNA. Each microarray comprised 770 317 distinct 25-mer probes to probe an estimated 28 853 transcripts, with a median 27 probes per gene. Gene expression changes that were associated with cardiac-specific *Kcne2* deletion were analyzed using *Ingenuity Pathway Analysis* (Qiagen, Hilden, Germany) to identify biological networks, pathways, processes, and diseases that were most highly represented in the differentially expressed gene (DEGs) identified. Expression changes of ≥1.5-fold and $P < .05$ were included in the analysis.

2.6 | Conventional PCR and real-time qPCR

For genotyping PCR, we used the primers listed in Table S3. Total RNA of the mouse left ventricle from 3 to 4-month-old mice was isolated and purified using the RNeasy Mini kit (Qiagen), followed by cDNA synthesis using the High Capacity cDNA Reverse Transcription Kit according to the manufacturer's instruction (Applied Biosystems, Foster City, CA, USA). Primers (FAM and TAMRA labels) utilized for quantifying transcript remodeling were purchased from Applied Biosystems and are listed in Table S4, except for 18s RNA (BioTez GmbH). The probe set for 18s RNA was the following: ACATCCAAGGAAGGCAGCAG (forward), TTTTCGTCACTACCTCCCCG (reverse), and FAMCGCGCAAATTACCCACTCCCGAC-TAMRA (probe). For amplification reaction, we used TaqMan Environmental Master Mix 2.0. For analysis we used REST software. For SYBR Green PCR we used Power SYBR Green PCR Master Mix and *Kcne2* and *Gapdh* primer sets (Bio Tez GmbH, Table S3).

2.7 | Immunofluorescence analysis

Ventricular cardiomyocytes were isolated and seeded as described previously[42] and fixed in 4% of PFA. Eight-µm cryo-sections from snap-frozen tissue were used for staining and fixed with ice-cooled acetone for 10 minutes. After fixation, cells and sections were blocked and permeabilized in 10% of serum (goat or donkey), 0.3% of Triton X-100, 0.2% of BSA for 1 hour, before overnight incubation at 4°C with primary antibodies (Table S5). Secondary antibodies used were Alexa-Fluor555 goat anti-rabbit, AlexaFluor647 goat anti-mouse (1:1000), or AlexaFluor488 goat anti-chicken. To stain nuclei we used DAPI (1:1000), wheat germ agglutinin AlexaFluorA555 (1:500) or phalloidin AlexaFluorA488 (1:500). For Kcne2 staining, we used a donkey anti-goat biotin-conjugated secondary antibody following by streptavidin AlexaFlourA555 (1:500). All listed fluorescent antibodies and reagents were purchased from Invitrogen (Carlsbad, USA) and were incubated for 60 minutes at RT. Stained cells and respectively cryo-sections were mounted with fluorescent mounting medium (Dako Cytomation, Carpinteria, USA) and imaged on confocal laser scanning microscope (TSC SP5 Leica Microsystems with software version LAS AF 2.632, Wetzlar, Deutschland). Images were assembled using Photoshop CS4 and CorelDRAW X4.

2.8 | Histology and electron microscopy

Hearts and lungs were dissected, rinsed in PBS, fixed overnight in phosphate-buffered 4% of paraformaldehyde (PFA), dehydrated successively in an alcohol series with increasing concentrations of ethanol, and embedded in paraffin. Five-µm sections were deparaffinized and stained with Masson`s Trichrome (Sigma-Aldrich, Saint Louis, USA) or H&E using standard procedures. Electron microscopy was performed as previously described.[40]

2.9 | Microbiome analysis

Stool samples were collected from male and female mice of ages 10–22 months (mean of three stool samples collected over a 24 hour period per mouse before and after 1 month treatments of proglumide or omeprazole), and then stored at −80°C until all samples were ready for sequencing. Except for two individuals, genotypes were not mixed in the same cage. All mice used for microbiome studies were housed in the same room in UC Irvine animal housing facilities. The sample DNA was isolated using the Zymobiomics DNA mini kit from Zymo Research. 16S rRNA amplicon PCR was performed targeting the V4-V5 region using the EMP primers (515F (barcoded) and 926R).[43,44] The library was sequenced at the UC Irvine Genomics High-Throughput Facility using a miseq v3 chemistry with a PE300 sequencing length. Sequencing resulted in 21.9 M reads passing filter (of which 18.4% are PhiX) with and overall Q30 > 76.7%. The raw sequences were imported into qiime2 (qiime2. org); 14.3 M paired end reads were binned into the designated barcodes. All samples (including the mock) showed abundant reads. After initial sample quality check and trimming (DADA2 in qiime2) there were 7.89 million paired end reads. These reads were used for further analysis. From the sequences the first 5 bp were trimmed and the forward read truncated at 299 bp, the reverse read at 238 bp. The sequences were assigned a taxonomic classification using the May 2013 “greengenes” database (greengenes.secondgenome.com), trained with the primer pairs that were used to amplify the 16S region.

2.10 | Data analysis and statistics

For statistical analysis other than for microbiome studies, Prism 5.0 software (GraphPad Software, Inc) was used. Results are presented as means ± SEM. Statistics was generally analyzed using Student's *t* test or two-way ANOVA followed by Bonferroni. For microbiome studies, statistical analyses were performed in R studio using the vegan, ggplot2, Ecolutils, and biomformat packages (all open source). Shannon diversity analysis was used to quantify alpha-diversity. Bray-Curtis distance matrices were used to calculate beta-diversity. The most influential bacteria types with respect to explaining gut microbiome differences between groups were identified using Simper (Similarity-percentage) analysis with Bray-Curtis dissimilarities.

3 | RESULTS

3.1 | Kcne2$^{CS-/-}$ mice exhibit premature mortality

We generated a cardiac-specific *Kcne2* knockout (*Kcne*$^{lox/lox}$*MHC+*) strain, hereafter referred to for simplicity as *Kcne2*$^{CS-/-}$, using the Cre-loxP system. In the floxed allele, exon 2 of *Kcne2* is flanked by loxP-sites. Floxed mice were crossed with αMHC-Cre-mice, and cardiac Cre-expression resulted in recombination with deletion of exon 2; disruption of the *Kcne2* gene resulted in an inhibition of LacZ expression. The alpha-myosin-heavy-chain (αMHC)-Cre transgene is active from mid-gestation and restricts expression of the Cre-recombinase to cardiomyocytes (Figure 1A,B). We observed almost complete loss of *Kcne2* mRNA expression in ventricular tissue from *Kcne2*$^{CS-/-}$ mice (Figure 1C). Immunostaining for β-galactosidase (Figure 1D) and Kcne2 (Figure 1E) protein revealed similar loss of expression in *Kcne2*$^{CS-/-}$ ventricular cardiomyocytes. Unexpectedly, cardiac-specific *Kcne2* deletion resulted in a steep onset of death in the cohort at 6 months of age, with a median longevity of 28 weeks (Figure 1F).

3.2 | Cardiac-specific *Kcne2* deletion diminishes ventricular Kv currents

To elucidate the basis for the steep increase in mortality caused by cardiac-specific *Kcne2* deletion, we first quantified ventricular myocyte Kv currents at 3–4 months of age, a stage at which the mice exhibited no echocardiographic or other outward clinical abnormalities (Table S1). Peak Kv current densities were decreased in *Kcne2*$^{CS-/-}$ cardiomyocytes (15 cells, n = 5 mice) compared to *Kcne2*$^{CS+/+}$ mice (12 cells, n = 5 mice, $P < .05$) with the most robust effect at +60 mV (Figure 2A). Mean myocyte-membrane capacitances were not altered by cardiac-specific *Kcne2* deletion (*Kcne2*$^{CS+/+}$, 123 ± 5.6pF; *Kcne2*$^{CS-/-}$, 127 ± 7.1pF). Functional effects of cardiac-specific *Kcne2* deletion were further dissected pharmacologically as we described previously,[23] using Kv current inhibitors to specifically eliminate I_{to} (heteropodatoxin 2; HpTx2) (500 nmol/L) and I_{Kslow1} (4-aminopyridine; 4-AP) (50 μmol/L) (Figure 2B,C). The 4-AP-sensitive Kv current density was halved by cardiac-specific *Kcne2* deletion (at +60 mV, $P < .001$; Figure 2B). The HpTx2-sensitive current density was not reduced at positive voltages, but its voltage dependence of activation was negative-shifted by 20 mV (Figure 2C). Quantification of inactivation rate at 0 mV yielded a $\tau_{inactivation}$ of 95.6 ± 18.3 ms for MHC- vs 50.64 ± 7.0 ms for MHC + mice ($P = .03$). Thus, *Kcne2*$^{CS-/-}$ doubled inactivation rate and shifted activation by −20 mV, exactly as would be predicted for loss of Kcne2 from ventricular myocyte Kv4.2 channel complexes.[45]

Similar to our previous findings from *Kcne2*$^{Glo-/-}$ mice,[23] in *Kcne2*$^{CS-/-}$ mice we also observed reduced Kv1.5 protein at the intercalated discs (ICDs) (Figure 2D–F), explaining the reduced Kv1.5 current density.

3.3 | Cardiac-specific *Kcne2* deletion causes progressive bradycardia, AV-Block and electromechanical dissociation

Because their ventricular myocyte Kv current defects were quantitatively similar to those we previously observed in age-matched global *Kcne2*$^{Glo-/-}$ mice,[23] which we did not previously (albeit non-quantitatively) observe to exhibit such early mortality,[32] we postulated that LQTS-associated ventricular arrhythmias were unlikely to be the primary mechanism for early mortality in *Kcne2*$^{CS-/-}$ mice. This hypothesis was confirmed using 24-hour Holter monitoring. In the 5 days prior to death, *Kcne2*$^{CS-/-}$ mice at age 6 months initially displayed normal sinus rhythm with similar heart rate to that of *Kcne2*$^{CS+/+}$ mice, before the former descended into progressive bradycardia (Figure 3A–C). This transitioned from sinus bradycardia to progressive AV-block (I°, II° and finally III°) and finally broad and deformed QRS complexes as a sign of ventricular escape rhythm and electromechanical dissociation (Figure 3D). Rather than ventricular arrhythmogenesis arising primarily from delayed repolarization, these ECG findings are instead consistent with terminal HF.

3.4 | *Kcne2*$^{CS-/-}$ causes early-onset dilated cardiomyopathy-type transcript remodeling

Having eliminated the possibility of ventricular arrhythmias underlying early mortality in *Kcne2*$^{CS-/-}$ mice, we conducted unbiased transcriptomic analysis of ventricular tissue from mice at 3–4 months of age, to detect potential concerted transcript expression changes that might give clues as to the molecular basis for premature mortality. Using this approach, we uncovered extensive transcriptome remodeling highly suggestive of cardiomyopathy and early molecular remodeling prior to dilated cardiomyopathy (DCM), including a return to fetal gene programing and a shift to glycolytic metabolism (Figure 4A–C; Table S2; Figures S1 and S2). Because these changes were apparent at 3–4 months, in the absence of echocardiographic abnormalities (Table S1), it suggests they arose as a primary response to *Kcne2* deletion rather than secondarily as a response to DCM or HF. In particular, genes related to DCM were differentially expressed in the ventricles of *Kcne2*$^{CS-/-}$ mice, including dystrophin (*Dmd*, −2.18) (Table S2). Differentially expressed genes also included sarcomeric proteins myotilin (*Myot*, −1.8), and those known to play a role in initializing the fetal gene program,[46] including *ANP* (+1.57), skeletal α1-actin (+1.65), and the T-type Ca^{2+} channel α 1H subunit-encoding *Cacna1h* (+1.78).

In the failing heart, anaerobic glucose oxidation is increased and fatty acid oxidation inhibited.[47] Accordingly, in *Kcne2*$^{CS-/-}$ mouse ventricles, expression was altered of glucokinase (*Gck*, +2.39), phosphofructokinase (*Pfkp*, +1.54), and genes encoding enzymes involved in glycogen metabolism, including 6-phosphofructo-2-kinase/fructose-2,6-biphosphatase 1 (*Pfkfb1*, −1.71), or gluconeogenesis, including Aldolase B (*Aldob*, −1.86). Fatty acid synthase (*Fasn*, +1.69) was upregulated, presumably as a counterpart to fatty acid oxidation. Real-time qPCR analysis (Figure 4D) confirmed the key findings of the microarray analysis and uncovered downregulation of *Kcna5*, consistent

with the observed downregulation of I_{Kslow1}. We also confirmed downregulation of protein expression, but not altered localization, for dystrophin and myotilin (Figure 4E,F).

3.5 | *Kcne2*$^{CS-/-}$ causes early-onset DCM and terminal HF

Strikingly, but consistent with the Holter and transcriptomic findings, echocardiographic evaluation of *Kcne2*$^{CS-/-}$ mice at age ~25 weeks confirmed severe, early-onset DCM, characterized by severe chamber dilation and thinned ventricular walls (Figure 5A,B). *Kcne2*$^{CS-/-}$ mice also exhibited significant HF evidenced by severely reduced global systolic pump function at ~25 weeks (Figure 5B). ECG analysis of *Kcne2*$^{CS-/-}$ *mice* with HF indicated significant QRS prolongation in *Kcne2*$^{CS-/-}$ mice (age ~25 weeks) compared to *Kcne2*$^{CS+/+}$ littermates, which could reflect bundle branch block due to DCM and failing ventricles (Figure 5C,D). *Kcne2*$^{CS-/-}$ mice at ~25 weeks also exhibited signs of backward HF, defined as inability of the heart to pump sufficient blood unless heart filling pressures are abnormally high. These included manifestations consistent with severe global HF, including myocardial fibrosis, global heart dilation, pleural effusions, cardiomegaly, hepatomegaly, cirrhosis of the kidneys, and pulmonary edema (Figure 5E–I, and see Videos S1–S3). Finally, *Kcne2*$^{CS-/-}$ mice at ~25 weeks exhibited focal and diffuse stages of myofilament derangement and lysis in left ventricular muscle (Figure 5J), a lesion directly correlated to increased HF deaths in DCM patients.[48]

3.6 | *Kcne2*$^{Glo-/-}$ mice exhibit DCM, HF, and 49% mortality by 60 weeks of age

Having established that cardiac-specific *Kcne2* deletion causes early, terminal HF, we revisited the effects of global *Kcne2* deletion. We previously found that at 3–6 months of age, global *Kcne2* deletion reduces ventricular myocyte I_{to} and I_{Kslow} current density.[23] These defects did not prolong baseline QT_c, but predisposed to sevoflurane-induced LQTS, and the majority of mice lived well beyond 6 months of age (although we did not at that time perform quantitative survival analysis). We also previously qualitatively observed cases of cardiomegaly in 15-m-old *Kcne2*$^{Glo-/-}$ mice.[32] Here, we quantified these changes using echocardiography. While young *Kcne2*$^{Glo-/-}$ mice from heterozygous crosses had normal cardiac morphology and contractile function, and no baseline arrhythmias,[23] we found that 12–15-m-old *Kcne2*$^{Glo-/-}$ mice from heterozygous crosses exhibit severe cardiomegaly (Figure 6A). Transthoracic echocardiography revealed significant chamber dilation and HF, as evidenced by reduced left ventricular ejection fraction (LVEF) and fractional shortening (FS), in aging (12–15-m-old) *Kcne2*$^{Glo-/-}$ mice (Figure 6B–D).

We next performed quantitative survival analysis of *Kcne2*$^{Glo-/-}$ mice for the first time, finding that global *Kcne2* deletion, concomitant with causing HF in aging mice, also accelerated mortality. However, effects were delayed by 32 weeks compared to those of cardiac-specific *Kcne2* deletion (median longevity 60 weeks, compared to 28 weeks in *Kcne2*$^{CS-/-}$ mice, $P < .01$; Figure 6E). This result is highly unexpected, that is, cardiac-specific *Kcne2* deletion caused a similar but more severe phenotype, and much earlier terminal HF, than global *Kcne2* deletion. Because of its importance and the ubiquity of its expression, global *Kcne2* deletion causes multiple phenotypes not present in *Kcne2*$^{CS-/-}$ mice, all of which would either be expected to not alter HF onset (eg, increased

seizure susceptibility[38]) or to accelerate HF (eg, diabetes,[35] hypercholesterolemia,[36] atherosclerosis,[39] and hypothyroidism[32]).

3.7 | Effects of *Kcne2* deletion on ventricular myocyte L-type Ca^{2+} current

We next compared effects of global vs cardiac-specific *Kcne2* deletion on L-type Ca^{2+} current in ventricular myocytes. Both cardiac-specific and global *Kcne2* deletion increased inactivation time constants (slowed inactivation) of L-type Ca^{2+} currents in ventricular myocytes from 3 to 6-month-old mice ($P < .05$) (Figure 7A,B). Global *Kcne2* deletion increased peak Ca^{2+} current at baseline and after isoproterenol stimulation, in 3–6-month-old mice ($P < .05$). Cardiac-specific *Kcne2* deletion had similar effects although less pronounced at positive membrane potentials and failing to reach $P < .05$ (Figure 7C). Cardiac-specific *Kcne2* deletion also produced small (~2.5 mV) negative-shifts in the midpoint voltage dependence of L-type Ca^{2+} current activation compared to wild-type, although the physiological significance of this small shift is not known, and statistical analysis was not possible because curves were fit to mean data for greater fit accuracy (Figure 7D).

By 12–15 months of age, $Kcne2^{Glo-/-}$ mice showed decreased peak L-type Ca^{2+} current at baseline compared to wild-type ($P < .05$) (Figure 7E) while similar to younger mice, the inactivation time constant was increased by global *Kcne2* deletion ($P < .05$) (Figure 7F).

3.8 | Hypergastrinemia does not alter the time course of terminal HF caused by *Kcne2* deletion in mice

The other major phenotype caused by global *Kcne2* deletion is hypochlorhydria, which in turn causes hypergastrinemia in $Kcne2^{Glo-/-}$ mice.[33,34,49] Reduced gastric acid secretion, for example, due to use of proton-pump inhibitors (PPIs) can also cause changes in gut microbiota.[50,51] We therefore hypothesized that HF occurs later in $Kcne2^{Glo-/-}$ mice than in $Kcne2^{CS-/-}$ mice either because of hypergastrinemia or altered gut microbiota in the former. Interestingly, prior work suggested cardiac infusion of gastrin in pigs[52] or activating the gastrin/CCK receptor in rat heart[53] may have positive inotropic effects, so we tested this eventuality first. Serum gastrin was 10-fold elevated in $Kcne2^{Glo-/-}$ mice at 20 weeks compared to age-matched $Kcne2^{Glo+/+}$ littermates, but unexpectedly, by 60 weeks (the median longevity for $Kcne2^{Glo-/-}$ mice), their serum gastrin had returned to normal (Figure 8A). In contrast, no such pattern was observed for histamine or C-peptide (insulin) in $Kcne2^{Glo-/-}$ mice (Figure 8B,C). This suggested that hypergastrinemia might be protective in $Kcne2^{Glo-/-}$ mice. However, inhibiting gastrin receptors by treating $Kcne2^{Glo-/-}$ mice via drinking water with gastrin receptor antagonist proglumide (20 mg kg^{-1}) for a mean duration of 33 weeks did not alter mean longevity, suggesting against a protective role for hypergastrinemia in *Kcne2*-linked HF (Figure 8D).

3.9 | A hypochlorhydria-linked decrease in gut Bacteroidales species is associated with delay of terminal HF

We next quantified the effects of global *Kcne2* deletion on the gut microbiome using 16s next-generation sequencing followed by taxonomic classification. Global *Kcne2* deletion did not affect alpha diversity (ie, overall species diversity, or species richness) (Figure

9A). In contrast, global *Kcne2* deletion altered the beta diversity (ie, the abundance of some species relative to others, or the dissimilarity between two samples), evident by the relative lack of overlap between the untreated $Kcne2^{Glo+/+}$ and $Kcne2^{Glo-/-}$ groups in the Principal Coordinates Analysis (PCoA) plot (Figure 9B). The altered beta diversity was likely unrelated to hypergastrinemia, as the gastrin receptor antagonist, proglumide (20 mg kg^{-1}) had no effect on beta diversity in $Kcne2^{Glo-/-}$ mice (Figure 9B). Taxa analysis using the Qiime2 platform identified two specific effects of global *Kcne2* deletion—a relative decrease in abundance of a subset of Bacteroidales species (Figure 9C,D) and increased relative abundance of Lactobacillaceae; Figure 9E,F). Simper analysis in the R statistical package also identified the importance of Bacteroidales, in particular Bacteroidales f24–7, in generating the dissimilarity between wild-type and $Kcne2^{Glo-/-}$ mice (Table S6).

To determine which, if any, of the microbiome changes arose from impaired gastric acid secretion, we treated wild-type mice with omeprazole, a proton-pump inhibitor activated by the low pH of the gastric lumen, for 4 months, and then sequenced their gut microbiomes. Omeprazole treatment altered wild-type mouse gut microbiome beta diversity such that it now more resembled that of $Kcne2^{Glo-/-}$ mice (Figure 9B). Strikingly, omeprazole also decreased the relative abundance of the same Bacteroidales subset of which abundance was decreased by global Kcne2 deletion but did not alter the relative abundance of Lactobacillaceae (Figure 9C–F). These findings were supported by Simper analysis in the R package, which identified the importance of Bacteroidales f24–7 in generating the dissimilarity between untreated and omeprazole-treated mice (Table S7). In contrast, proglumide treatment did not alter the relative abundance of Bacteroidales or Lactobacillaceae (Figure 9C,E).

Gut Bacteroidales were recently found to be relatively enriched in people with a high lifetime cardiovascular risk profile,[54] suggesting the hypothesis that the reduced Bacteroidales in $Kcne2^{Glo-/-}$ mice contributes to the delay in terminal HF. We therefore examined the effects of omeprazole on longevity in $Kcne2^{CS-/-}$ mice. Strikingly, treatment of $Kcne2^{CS-/-}$ mice with omeprazole for 20 weeks beginning at mean age 24 weeks (ie, when HF is already apparent and mortality begins to accelerate) increased survival 10-fold, from 4% to 43%, at 44 weeks ($P < .05$), extending longevity to match that of $Kcne2^{Glo-/-}$ mice (Figure 10).

4 | DISCUSSION

Our findings support three unexpected conclusions. First, *Kcne2* deletion (cardiac-specific or global) causes DCM and terminal HF. Second, cardiac-specific *Kcne2* deletion (median survival 28 weeks) is more severe than global *Kcne2* deletion (median survival 60 weeks). Third, terminal HF is delayed in $Kcne2^{CS-/-}$ mice by administering omeprazole, which mimics the hypochlorhydria, decreased relative abundance of gut Bacteroidales and increased longevity induced by global *Kcne2* deletion.

Mutations in >50 genes have been associated with familial DCM, and disruption of ion channel function (observations of patients with ion channel mutations, and from transgenic mouse models), more often associated with arrhythmias, can cause cardiomyopathy and

HF. What makes the *Kcne2*$^{Glo-/-}$ mouse model unique is that in addition to directly causing HF via a myocyte-based mechanism (as evidenced by HF in *Kcne2*$^{CS-/-}$ mice), global *Kcne2* deletion also causes other HF risk factors, including hypercholesterolemia,[36] hyperhomocysteinemia, fatty liver,[37] atherosclerosis,[39] and type 2 diabetes.[35] Thus, *Kcne2*$^{Glo-/-}$ mice exhibit many features representative of the typical human HF scenario, including risk factors associated with myocardial ischemia, and also a progressive increase in severity of these factors, features important for the utility of animal HF models.[55] It is nonetheless important to note that human *KCNE2* sequence variation has not to date been associated with HF, and gene knockout in mice is a very different scenario to the typical substitutions observed in human gene sequence variation.

Interestingly, heterozygous *Scn5a*-knockout mice develop extensive myocardial fibrosis and upregulation of hypertrophic markers as they age. Nav1.5 interacts with cytoskeletal components such as the dystrophin protein complex[56] and it has been proposed that sodium channel mutations causing cardiomyopathy cause loss or weakening of such interactions. Additionally, the titin N-terminal domain binds to T-cap (telethonin) and the Kv channel β subunit KCNE1, within the Z-band region of the sarcomere.[57] This suggests a mechanistic link between structural proteins such as sarcomere proteins and ion channel proteins, potentially favoring the development of ventricular arrhythmias in patients with DCM.

The primary causes of DCM-associated arrhythmias are not well understood. In DCM, disruption of the link between the sarcolemma and the sarcomere has been shown to be associated with disease progression, whereas the “smoking gun” in rhythm disorders is disturbance of ion channel function.[54] Interestingly, Kv1.5 binds to the structural Z-band protein α-actinin.[56] Although Kv1.5 so far has not been linked to DCM, Kv1.5 currents could be affected in individuals with DCM harboring α-actinin mutations, thereby predisposing affected individuals to malignant ventricular arrhythmias and SCD. Here, we found that cardiac-specific *Kcne2* deletion reduces Kv1.5 protein expression at the ICDs (Figure 2D–F), as we previously observed in ventricular myocytes of global *Kcne2*$^{-/-}$ mice.[23] In contrast, in global *Kcne3*$^{-/-}$ mice, in which we observed neither DCM nor HF, hypoaldosteronism-dependent increase in Kv1.5 expression at the ICDs contributed to a reduced atrial refractory period and atrial fibrillation.[57]

Our microarray data clearly show sarcomeric and metabolic transcript remodeling, and a return to fetal gene reprograming, characteristic of DCM. However, we do not yet know whether this remodeling is directly triggered by a gene reprograming/transcriptional effect of *Kcne2* deletion, subsequently leading to DCM, or alternatively whether *Kcne2* deletion directly disrupts functionality of the sarcomere or other elements of the contractile apparatus, leading to the associated remodeling and ultimately DCM and HF. We do know that the molecular remodeling occurs before echocardiographic abnormalities are apparent and is not, therefore, secondary to structural changes in DCM. One possibility is that the increased *PFKFB1* expression we observe in *Kcne2*$^{CS-/-}$ mice contributes to myocyte dysfunction.[58] Another is that loss of Kcne2 interaction with filamin eliminates a protective mechanism and contributes to loss of myocyte structural integrity under hypoxic conditions, exacerbating HF following disease onset.[59]

Interestingly, in addition to its established role as a Kv channel ancillary subunit, *Kcne2* also regulates the cardiac L-type calcium channel, Cav1.2.[25] This is particularly relevant to the present study, because genetic manipulation of Cav1.2 (mutation of the IQ motif, abolishing calmodulin-dependent inactivation and facilitation) was previously found to induce lethal DCM in mice.[58] We found that both global and cardiac-specific *Kcne2* deletion increased peak L-type Ca^{2+} current in ventricular myocytes from young (3–6-month-old) mice, in line with the previously reported effects of Kcne2 knockdown[25]; interestingly, this had reversed by 12–15 months in $Kcne2^{Glo-/-}$ mice, suggestive of opposite remodeling later in life. In addition, we found that both cardiac-specific and global *Kcne2* deletion slowed L-type Ca^{2+} channel inactivation, regardless of age, which could contribute to greater cytosolic Ca^{2+} accumulation or disrupt timing of other processes, as could the negative shift in the voltage dependence of L-type calcium channel activation we observed. Thus, it is possible that loss of specific aspects of Cav1.2 regulation at least contributes to early lethal DCM/HF in cardiac-specific $Kcne2^{-/-}$ mice.

New therapeutic approaches to HF are urgently warranted, given the increasingly large burden it places on quality of life and healthcare systems worldwide. Previously, intracoronary infusion of gastrin was found to increase cardiac output in pigs,[52] and increased serum gastrin levels were tentatively associated with decreased cardiovascular mortality in an elderly human cohort.[59] Here, we essentially ruled out hypergastrinemia as a factor in the hypochlorhydria-linked HF delay because proglumide did not reduce longevity. Instead, we found that similar gut microbiome changes were caused by $Kcne2^{Glo-/-}$ or by omeprazole treatment, either of which delayed terminal HF compared to untreated $Kcne2^{CS-/-}$ mice. To our knowledge, the current study is the first to demonstrate a therapeutic effect of genetically or pharmacologically induced hypochlorhydria in HF. The only detectable change in gut flora common to both pharmacologic and genetically induced hypochlorhydria was a decrease in the relative abundance of Bacteroidales (especially f24–7), which constitute a major bacterial order in human gastrointestinal gut flora.

There is currently much interest in understanding the role of gut flora in human health and disease. Bacteroidales were recently found to be relatively more abundant in the GI tracts of people with a higher lifetime cardiovascular risk profile,[54] suggesting that reduced Bacteroidales abundance might be beneficial at least in some contexts. In a study of elderly Chinese, reduced Bacteroidales abundance was found in those on a high-fiber diet.[60] In a recent meta-analysis incorporating almost 135 million person-years of data, the highest-fiber diet was associated with 15%−30% decreased all-cause and cardiovascular related mortality, further cementing the health value of dietary fiber.[61] In mice, the relative abundance of gut Bacteroidales was higher in mice administered *Porphyromonas gingivalis* to mimic gum disease; the higher Bacteroidales also associated with insulin resistance and systemic inflammation.[62] Furthermore, raspberries, a fruit rich in phenolic and polyphenolic compounds and consumption of which confers numerous cardiovascular benefits in mice and people[63] were recently also found to decrease the relative abundance of gut Bacteroidales in obese diabetic mice.[64]

Our findings in mice of the apparent benefits of omeprazole in HF reflect findings in some human studies, although there is not absolute consensus in clinical studies. In a recent study

of 1191 HF patients, proton-pump inhibitor (PPI) use was associated with better outcome compared to the nonacid suppressive therapy group or to the group taking histamine H_2 receptor antagonists (H2RAs).[65] In other studies, omeprazole was not found to alter cardiovascular event risk in high-risk cardiovascular patients,[66] nor did omeprazole increase mortality in coronary angioplasty patients concomitantly taking clopidogrel.[67] Furthermore, esomeprazole has been shown to decrease blood pressure and endothelial dysfunction and exhibit antioxidant and anti-inflammatory actions in human tissues and animal models.[68] In contrast, in a study of 42902 PPI initiators vs 3296 histamine H_2 receptor antagonist (H2RA) initiators, H2RA use was associated with lower mortality in HF patients than was PPI use.[69] In a study of 706 patients, PPI use was associated with increased HF incidence and mortality[70]; in a study of all-cause mortality associated with taking PPIs conducted in more than 200 000 US veterans, PPI use was associated with a “small excess” of cause-specific mortality including deaths from cardiovascular disease.[71]

If the positive effects we observe in mice are repeated in a large animal model, the possibility of assessing the worth of altering the gut microbiome for HF patients could be considered, perhaps with dietary modifications or fecal transplantation rather than with PPIs, given the potential health concerns. While we do not yet understand the molecular basis for hypochlorhydria-associated cardioprotection, including the importance of gut microbiome changes and the potential gastric vs non-gastric benefits of omeprazole, one possible factor is constitutive induction of the cardioprotective RISK pathway, which we previously observed in *Kcne2*$^{\mathrm{Glo}-/-}$ mice.[72]

Supplementary Material

Refer to Web version on PubMed Central for supplementary material.

ACKNOWLEDGMENTS

We thank Aidi Cao, Carolin Gaertner, Nora Lange, and members of the telemetry and echocardiography facility, especially Ilona Kamer, Martin Taube, and Stefanie Schelenz for excellent technical expertise (ECRC, Berlin, Germany). We thank Lily Chen (UC Irvine) for technical assistance. We are grateful for a University of California, Irvine Microbiome Initiative Pilot Project Award for microbiome sequencing and analysis. We thank Drs. Jennifer Martiny, Claudia Weihe, and Julio Avelar-Barragan (UC Irvine) for microbiome sequencing, training and advice on sequence data analysis.

Funding information

The Deutsche Forschungsgemeinschaft, Fritz-Thyssen-Stiftung, and intramural ECRC funding (to TKR), US National Institutes of Health (GM115189, GM130377, and DK041544 to GWA), and a UC Irvine Microbiome Initiative Pilot Project Award (to GWA) supported this work

Abbreviations:

4-AP
4-aminopyridine

AV
atrioventricular

DCM

dilative cardiomyopathy

HF
heart failure

HpTx2
heteropodatoxin 2

ICD
intercalated disc

Kcne2 **$^{CS-/-}$**
cardiac-specific *Kcne2* knockout

Kcne2 **$^{Glo-/-}$**
global *Kcne2* knockout

LQTS
long QT syndrome

MHC
myosin heavy chain

SCD
sudden cardiac death

REFERENCES

1. Cohn JN, Archibald DG, Ziesche S, et al. Effect of vasodilator therapy on mortality in chronic congestive heart failure. Results of a Veterans Administration Cooperative Study. N Engl J Med. 1986;314:1547–1552. 10.1056/NEJM198606123142404 [PubMed: 3520315]
2. Stevenson WG, Stevenson LW, Middlekauff HR, Saxon LA. Sudden death prevention in patients with advanced ventricular dysfunction. Circulation. 1993;88:2953–2961. [PubMed: 8252708]
3. Roger VL. Epidemiology of heart failure. Circ Res. 2013;113:646–659. 10.1161/CIRCRESAHA.113.300268 [PubMed: 23989710]
4. Ziaeian B, Fonarow GC. Epidemiology and aetiology of heart failure. Nat Rev Cardiol. 2016;13:368–378. 10.1038/nrcardio.2016.25 [PubMed: 26935038]
5. Mozaffarian D, Benjamin EJ, Go AS, et al. Heart disease and stroke statistics-2016 update: a report from the American Heart Association. Circulation. 2016;133:e38–e360. 10.1161/CIR.0000000000000350 [PubMed: 26673558]
6. Curran ME, Splawski I, Timothy KW, et al. A molecular basis for cardiac arrhythmia: HERG mutations cause long QT syndrome. Cell. 1995;80:795–803. [PubMed: 7889573]
7. Wang Q, et al. SCN5A mutations associated with an inherited cardiac arrhythmia, long QT syndrome. Cell. 1995;80:805–811. [PubMed: 7889574]
8. Neyroud N, Tesson F, Denjoy I, et al. A novel mutation in the potassium channel gene KVLQT1 causes the Jervell and Lange-Nielsen cardioauditory syndrome. Nat Genet. 1997;15:186–189. 10.1038/ng0297-186 [PubMed: 9020846]
9. Abbott GW. KCNE genetics and pharmacogenomics in cardiac arrhythmias: much ado about nothing? Expert Rev Clin Pharmacol. 2013;6:49–60. 10.1586/ecp.12.76 [PubMed: 23272793]
10. Abbott GW, Sesti F, Splawski I, et al. MiRP1 forms IKr potassium channels with HERG and is associated with cardiac arrhythmia. Cell. 1999;97:175–187. [PubMed: 10219239]

11. Splawski I, Tristani-Firouzi M, Lehmann MH, Sanguinetti MC, Keating MT. Mutations in the hminK gene cause long QT syndrome and suppress IKs function. Nat Genet. 1997;17:338–340. 10.1038/ng1197-338 [PubMed: 9354802]
12. Abbott GW. The KCNE2 K(+) channel regulatory subunit: Ubiquitous influence, complex pathobiology. Gene. 2015;569:162–172. 10.1016/j.gene.2015.06.061 [PubMed: 26123744]
13. Roepke TK, Abbott GW. Pharmacogenetics and cardiac ion channels. Vascul Pharmacol. 2006;44:90–106. 10.1016/j.vph.2005.07.013 [PubMed: 16344000]
14. Gordon E, Panaghie G, Deng L, et al. A KCNE2 mutation in a patient with cardiac arrhythmia induced by auditory stimuli and serum electrolyte imbalance. Cardiovasc Res. 2008;77:98–106. 10.1093/cvr/cvm030 [PubMed: 18006462]
15. Sesti F, Abbott GW, Wei J, et al. A common polymorphism associated with antibiotic-induced cardiac arrhythmia. Proc Natl Acad Sci U S A. 2000;97:10613–10618. 10.1073/pnas.180223197 [PubMed: 10984545]
16. Lewis A, McCrossan ZA, Abbott GW. MinK, MiRP1, and MiRP2 diversify Kv3.1 and Kv3.2 potassium channel gating. J Biol Chem. 2004;279:7884–7892. 10.1074/jbc.M310501200 [PubMed: 14679187]
17. Abbott GW, Butler MH, Bendahhou S, et al. MiRP2 forms potassium channels in skeletal muscle with Kv3.4 and is associated with periodic paralysis. Cell. 2001;104:217–231. [PubMed: 11207363]
18. McCrossan ZA, Roepke TK, Lewis A, Panaghie G, Abbott GW. Regulation of the Kv2.1 potassium channel by MinK and MiRP1. J Membr Biol. 2009;228:1–14. 10.1007/s00232-009-9154-8 [PubMed: 19219384]
19. Roepke TK, Kanda VA, Purtell K, et al. KCNE2 forms potassium channels with KCNA3 and KCNQ1 in the choroid plexus epithelium. FASEB J. 2011;25:4264–4273. [PubMed: 21859894]
20. Tinel N, Diochot S, Borsotto M, Lazdunski M, Barhanin J. KCNE2 confers background current characteristics to the cardiac KCNQ1 potassium channel. EMBO J. 2000;19:6326–6330. 10.1093/emboj/19.23.6326 [PubMed: 11101505]
21. Kanda VA, Lewis A, Xu X, Abbott GW. KCNE1 and KCNE2 provide a checkpoint governing voltage-gated potassium channel alpha-subunit composition. Biophys J. 2011;101:1364–1375. 10.1016/j.bpj.2011.08.014 [PubMed: 21943417]
22. Kanda VA, Lewis A, Xu X, Abbott GW. KCNE1 and KCNE2 inhibit forward trafficking of homomeric N-type voltage-gated potassium channels. Biophys J. 2011;101:1354–1363. 10.1016/j.bpj.2011.08.015 [PubMed: 21943416]
23. Roepke TK, Kontogeorgis A, Ovanez C, et al. Targeted deletion of kcne2 impairs ventricular repolarization via disruption of I(K, slow1) and I(to, f). FASEB J. 2008;22:3648–3660. 10.1096/fj.08-110171 [PubMed: 18603586]
24. Qu J, Kryukova Y, Potapova IA, et al. MiRP1 modulates HCN2 channel expression and gating in cardiac myocytes. J Biol Chem. 2004;279:43497–43502. 10.1074/jbc.M405018200 [PubMed: 15292247]
25. Liu W, Deng J, Wang G, et al. KCNE2 modulates cardiac L-type Ca2+ channel, Journal of Molecular and Cellular Cardiology. 2014;72:208–218. 10.1016/j.yjmcc.2014.03.013 [PubMed: 24681347]
26. Bendahhou S, Marionneau C, Haurogne K, et al. In vitro molecular interactions and distribution of KCNE family with KCNQ1 in the human heart. Cardiovasc Res. 2005;67:529–538. 10.1016/j.cardiores.2005.02.014 [PubMed: 16039274]
27. Radicke S, Cotella D, Graf EM, et al. Functional modulation of the transient outward current Ito by KCNE beta-subunits and regional distribution in human non-failing and failing hearts. Cardiovasc Res. 2006;71:695–703. 10.1016/j.cardiores.2006.06.017 [PubMed: 16876774]
28. Sabater-Lleal M, Mälarstig A, Folkersen L, et al. Common genetic determinants of lung function, subclinical atherosclerosis and risk of coronary artery disease. PLoS One. 2014;9:e104082. 10.1371/journal.pone.0104082 [PubMed: 25093840]
29. Wakil SM, Ram R, Muiya NP, et al. A genome-wide association study reveals susceptibility loci for myocardial infarction/coronary artery disease in Saudi Arabs. Atherosclerosis. 2016;245:62–70. 10.1016/j.atherosclerosis.2015.11.019 [PubMed: 26708285]

30. Kathiresan S, Voight BF, Purcell S, et al. Genome-wide association of early-onset myocardial infarction with single nucleotide polymorphisms and copy number variants. Nat Genet. 2009;41:334–341. 10.1038/ng.327 [PubMed: 19198609]

31. Szpakowicz A, Kiliszek M, Pepinski W, et al. The rs9982601 polymorphism of the region between the SLC5A3/MRPS6 and KCNE2 genes associated with a prevalence of myocardial infarction and subsequent long-term mortality. Pol Arch Med Wewn. 2015;125:240–248. [PubMed: 25697262]

32. Roepke TK, King EC, Reyna-Neyra A, et al. Kcne2 deletion uncovers its crucial role in thyroid hormone biosynthesis. Nat Med. 2009;15:1186–1194. 10.1038/nm.2029 [PubMed: 19767733]

33. Roepke TK, Anantharam A, Kirchhoff P, et al. The KCNE2 potassium channel ancillary subunit is essential for gastric acid secretion. J Biol Chem. 2006;281:23740–23747. 10.1074/jbc.M604155200 [PubMed: 16754665]

34. Roepke TK, King EC, Purtell K, et al. Genetic dissection reveals unexpected influence of beta subunits on KCNQ1 K+ channel polarized trafficking in vivo. FASEB J. 2011;25:727–736. 10.1096/fj.10-173682 [PubMed: 21084694]

35. Lee SM, Baik J, Nguyen D, et al. Kcne2 deletion impairs insulin secretion and causes type 2 diabetes mellitus. FASEB J 2017;31:2674–2685. 10.1096/fj.201601347 [PubMed: 28280005]

36. Hu Z, et al. Kcne2 deletion creates a multisystem syndrome predisposing to sudden cardiac death. Circ Cardiovasc Genet. 2014;7:33–42. 10.1161/CIRCGENETICS.113.000315 [PubMed: 24403551]

37. Lee SM, Nguyen D, Anand M, et al. Kcne2 deletion causes early-onset nonalcoholic fatty liver disease via iron deficiency anemia. Sci Rep. 2016;6:23118. 10.1038/srep23118 [PubMed: 26984260]

38. Abbott GW, Tai K-K, Neverisky Dl, et al. KCNQ1, KCNE2, and Na+-coupled solute transporters form reciprocally regulating complexes that affect neuronal excitability. Sci Signal, 2014;7:ra22. 10.1126/scisignal.2005025 [PubMed: 24595108]

39. Lee SM, Nguyen D, Hu Z, Abbott GW. Kcne2 deletion promotes atherosclerosis and diet-dependent sudden death. J Mol Cell Cardiol. 2015;87:148–151. 10.1016/j.yjmcc.2015.08.013 [PubMed: 26307149]

40. Lisewski U, Shi YU, Wrackmeyer U, et al. The tight junction protein CAR regulates cardiac conduction and cell-cell communication. J Exp Med. 2008;205:2369–2379. 10.1084/jem.20080897 [PubMed: 18794341]

41. Mongue-Din H, Salmon A, Fiszman MY, Fromes Y. Non-invasive restrained ECG recording in conscious small rodents: a new tool for cardiac electrical activity investigation. Pflugers Arch. 2007;454:165–171. 10.1007/s00424-006-0197-8 [PubMed: 17226051]

42. Köhncke C, Lisewski U, Schleußner L, et al. Isolation and Kv channel recordings in murine atrial and ventricular cardiomyocytes. J Vis Exp. 2013:e50145. 10.3791/50145 [PubMed: 23524949]

43. Caporaso JG, Lauber CL, Walters WA, et al. Ultra-high-throughput microbial community analysis on the Illumina HiSeq and MiSeq platforms. ISME J. 2012;6:1621–1624. 10.1038/ismej.2012.8 [PubMed: 22402401]

44. Walters W, Hyde ER, Berg-Lyons D, et al. Improved bacterial 16S rRNA Gene (V4 and V4–5) and fungal internal transcribed spacer marker gene primers for microbial community surveys. mSystems. 2016;1:e00009–e00015. 10.1128/mSystems.00009-15

45. Zhang M, Jiang M, Tseng GN. minK-related peptide 1 associates with Kv4.2 and modulates its gating function: potential role as beta subunit of cardiac transient outward channel? Circ Res. 2001;88:1012–1019. [PubMed: 11375270]

46. Kuwahara K, Nishikimi T, Nakao K. Transcriptional regulation of the fetal cardiac gene program. J Pharmacol Sci. 2012;119:198–203. [PubMed: 22786561]

47. Calmettes G, Ribalet B, John S, et al. Hexokinases and cardioprotection. J Mol Cell Cardiol. 2015;78:107–115. 10.1016/j.yjmcc.2014.09.020 [PubMed: 25264175]

48. Saito T, Asai K, Sato S, et al. Ultrastructural features of cardiomyocytes in dilated cardiomyopathy with initially decompensated heart failure as a predictor of prognosis. Eur Heart J. 2015;36:724–732. 10.1093/eurheartj/ehu404 [PubMed: 25336212]

49. Roepke TK, Purtell K, King EC, et al. Targeted deletion of Kcne2 causes gastritis cystica profunda and gastric neoplasia. PLoS One. 2010;5:e11451. 10.1371/journal.pone.0011451 [PubMed: 20625512]
50. Garcia-Mazcorro JF, Suchodolski JS, Jones KR, et al. Effect of the proton pump inhibitor omeprazole on the gastrointestinal bacterial microbiota of healthy dogs. FEMS Microbiol Ecol. 2012;80:624–636. 10.1111/j.1574-6941.2012.01331.x [PubMed: 22324305]
51. Hojo M, Asahara T, Nagahara A, et al. Gut microbiota composition before and after use of proton pump inhibitors. Dig Dis Sci. 2018;63:2940–2949. 10.1007/s10620-018-5122-4 [PubMed: 29796911]
52. Grossini E, Caimmi P, Molinari C, et al. Intracoronary gastrin 17 increases cardiac perfusion and function through autonomic nervous system, CCK receptors, and nitric oxide in anesthetized pigs. J Appl Physiol. 2011;1985(110):95–108. 10.1152/japplphysiol.00625.2010
53. Zhao XY, Ling YL, Li YG, Meng AH, Xing HY. Cholecystokinin octapeptide improves cardiac function by activating cholecystokinin octapeptide receptor in endotoxic shock rats. World J Gastroenterol. 2005;11:3405–3410. [PubMed: 15948246]
54. Kelly TN, Bazzano LA, Ajami NJ, et al. Gut microbiome associates with lifetime cardiovascular disease risk profile among bogalusa heart study participants. Circ Res. 2016;119:956–964. 10.1161/CIRCRESAHA.116.309219 [PubMed: 27507222]
55. Houser SR, Margulies KB, Murphy AM, et al. Animal models of heart failure: a scientific statement from the American Heart Association. Circ Res. 2012;111:131–150. 10.1161/RES.0b013e3182582523 [PubMed: 22595296]
56. Gavillet B, Rougier J-S, Domenighetti AA, et al. Cardiac sodium channel Nav1.5 is regulated by a multiprotein complex composed of syntrophins and dystrophin. Circ Res. 2006;99:407–414. 10.1161/01.RES.0000237466.13252.5e [PubMed: 16857961]
57. Furukawa T, Ono Y, & Tsuchiya H, et al. Specific interaction of the potassium channel beta-subunit minK with the sarcomeric protein T-cap suggests a T-tubule-myofibril linking system. J Mol Biol. 2001;313:775–784. 10.1006/jmbi.2001.5053 [PubMed: 11697903]
58. Blaich A, Pahlavan S, Tian Q, et al. Mutation of the calmodulin binding motif IQ of the L-type Ca(v)1.2 Ca2+ channel to EQ induces dilated cardiomyopathy and death. J Biol Chem. 2012;287:22616–22625. 10.1074/jbc.M112.357921 [PubMed: 22589547]
59. Goetze JP, Rehfeld JF, Alehagen U. Cholecystokinin in plasma predicts cardiovascular mortality in elderly females. Int J Cardiol. 2016;209:37–41. 10.1016/j.ijcard.2016.02.038 [PubMed: 26878472]
60. Wang F, Yu T, Huang G, et al. Gut microbiota community and its assembly associated with age and diet in chinese centenarians. J Microbiol Biotechnol. 2015;25:1195–1204. 10.4014/jmb.1410.10014 [PubMed: 25839332]
61. Reynolds A, Mann J, Cummings J, et al. Carbohydrate quality and human health: a series of systematic reviews and meta-analyses. Lancet. 2019;393:434–445. 10.1016/S0140-6736(18)31809-9 [PubMed: 30638909]
62. Arimatsu K, Yamada H, Miyazawa H, et al. Oral pathobiont induces systemic inflammation and metabolic changes associated with alteration of gut microbiota. Sci Rep. 2014;4:4828. 10.1038/srep04828 [PubMed: 24797416]
63. Burton-Freeman BM, Sandhu AK, Edirisinghe I. Red raspber-ries and their bioactive polyphenols: cardiometabolic and neuronal health links. Adv Nutr. 2016;7:44–65. 10.3945/an.115.009639 [PubMed: 26773014]
64. Garcia-Mazcorro JF, Pedreschi R, Chew B, et al. Dietary supplementation with raspberry extracts modifies the fecal microbiota in obese diabetic db/db mice. J Microbiol Biotechnol. 2018;28:1247–1259. 10.4014/jmb.1803.03020 [PubMed: 29943551]
65. Yoshihisa A, Takiguchi M, Kanno Y, et al. Associations of acid suppressive therapy with cardiac mortality in heart failure patients. J Am Heart Assoc. 2017;6:e005110. 10.1161/JAHA.116.005110 [PubMed: 28512114]
66. Vaduganathan M, Cannon CP, Cryer BL, et al. Efficacy and safety of proton-pump inhibitors in high-risk cardiovascular subsets of the COGENT trial. Am J Med. 2016;129:1002–1005. 10.1016/j.amjmed.2016.03.042 [PubMed: 27143321]

67. Bundhun PK, Teeluck AR, Bhurtu A, Huang WQ. Is the concomitant use of clopidogrel and Proton Pump Inhibitors still associated with increased adverse cardiovascular outcomes following coronary angioplasty?: a systematic review and meta-analysis of recently published studies (2012–2016). BMC Cardiovasc Disord. 2017;17:3. 10.1186/s12872-016-0453-6 [PubMed: 28056809]

68. Onda K, Tong S, Beard S, et al. Proton pump inhibitors decrease soluble fms-like tyrosine kinase-1 and soluble endoglin secretion, decrease hypertension, and rescue endothelial dysfunction. Hypertension. 2017;69:457–468. 10.1161/HYPERTENSIONAHA.116.08408 [PubMed: 28115513]

69. Adelborg K, et al. Use of histamine H2 receptor antagonists and outcomes in patients with heart failure: a nationwide population-based cohort study. Clin Epidemiol. 2018;10:521–530. 10.2147/CLEP.S162909 [PubMed: 29765253]

70. Pello Lázaro AM, Cristóbal C, Franco-Peláez JA, et al. Use of proton-pump inhibitors predicts heart failure and death in patients with coronary artery disease. PLoS One. 2017;12:e0169826. 10.1371/journal.pone.0169826 [PubMed: 28103324]

71. Xie Y, Bowe B, Yan Y, et al. Estimates of all cause mortality and cause specific mortality associated with proton pump inhibitors among US veterans: cohort study. BMJ. 2019;365:l1580. 10.1136/bmj.l1580 [PubMed: 31147311]

72. Hu Z, Crump SM, Zhang P, Abbott GW. Kcne2 deletion attenuates acute post-ischaemia/reperfusion myocardial infarction. Cardiovasc Res. 2016;110:227–237. 10.1093/cvr/cvw048 [PubMed: 26952045]

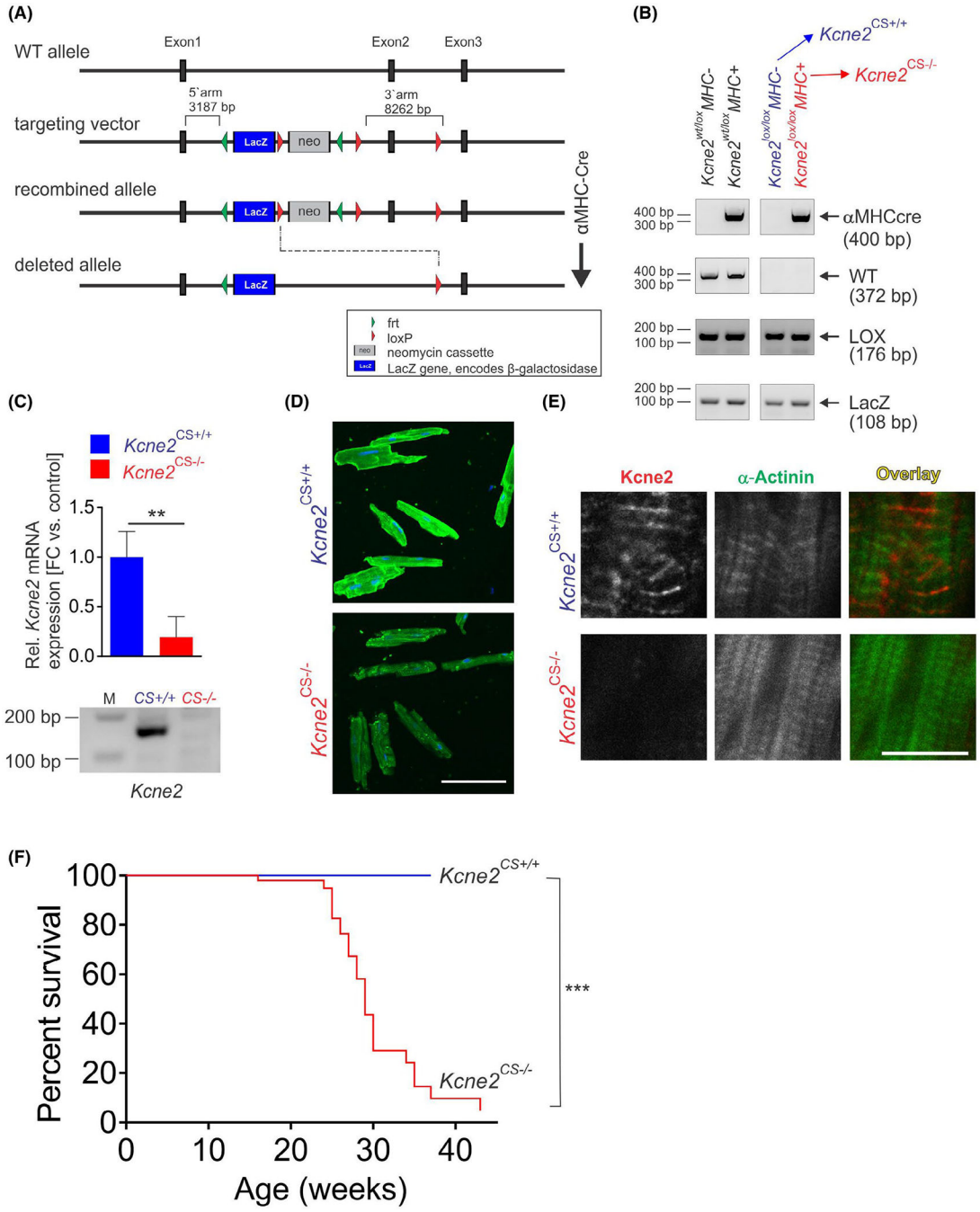

FIGURE 1.

Cardiac-specific *Kcne2* knockout causes early mortality. A, Targeting strategy using the Cre-loxP system. Wild-type (WT) allele is shown with exons depicted as black boxes. The targeting construct contains a neomycin cassette (neo) and LacZ gene (LacZ), flanked by frt and loxP sites. A mouse line expressing Cre-recombinase under the control of the αMHC (alpha myosin heavy chain) promoter was used to generate a heart-specific *Kcne2* knockout strain (*Kcne2*$^{CS-/-}$ mice). Cardiac Cre-expression results in recombination with deletion of exon 2 and inactivation of *Kcne2* by frameshift. B, Examples of genotype PCRs

of heterozygous (wt/lox) and homozygous (lox/lox) Cre^{-} and Cre^{+} animals. Mice can be genotyped through a combination of separate PCR reactions that detect Cre-recombinase (400 bp), LacZ (108 bp), the gene-specific wild-type allele (372 bp), a mutant allele-specific short range PCR (Lox, 176 bp). Note, the WT allele is only detectable in heterozygous, but not in homozygous animals. C, Quantitative real-time PCR (upper) and PCR-product agarose gel (lower) of $Kcne2^{CS+/+}$ vs $Kcne2^{CS-/-}$ ventricles. D, Immunofluorescence with specific antibody against β-Gal (green) revealed signal in $Kcne2^{CS+/+}$, but not in $Kcne2^{CS-/-}$ mouse cardiomyocytes. Bar = 75 μm. DAPI was used to stain nuclei (blue). E, Immunofluorescence with specific antibody against *Kcne2* (red) revealed signal in $Kcne2^{CS+/+}$, but not $Kcne2^{CS-/-}$ cardiomyocytes. Anti-α-actinin-antibody (green) was used to stain z-disc of sarcomeres. Bar = 20 μm. F, Kaplan-Meier survival curve demonstrating a significant increase in spontaneous death in $Kcne2^{CS-/-}$ mice (red) compared to their $Kcne2^{CS+/+}$ littermates (blue) (n = 25–33 mice per group at time-point zero) $^{***}P < .001$

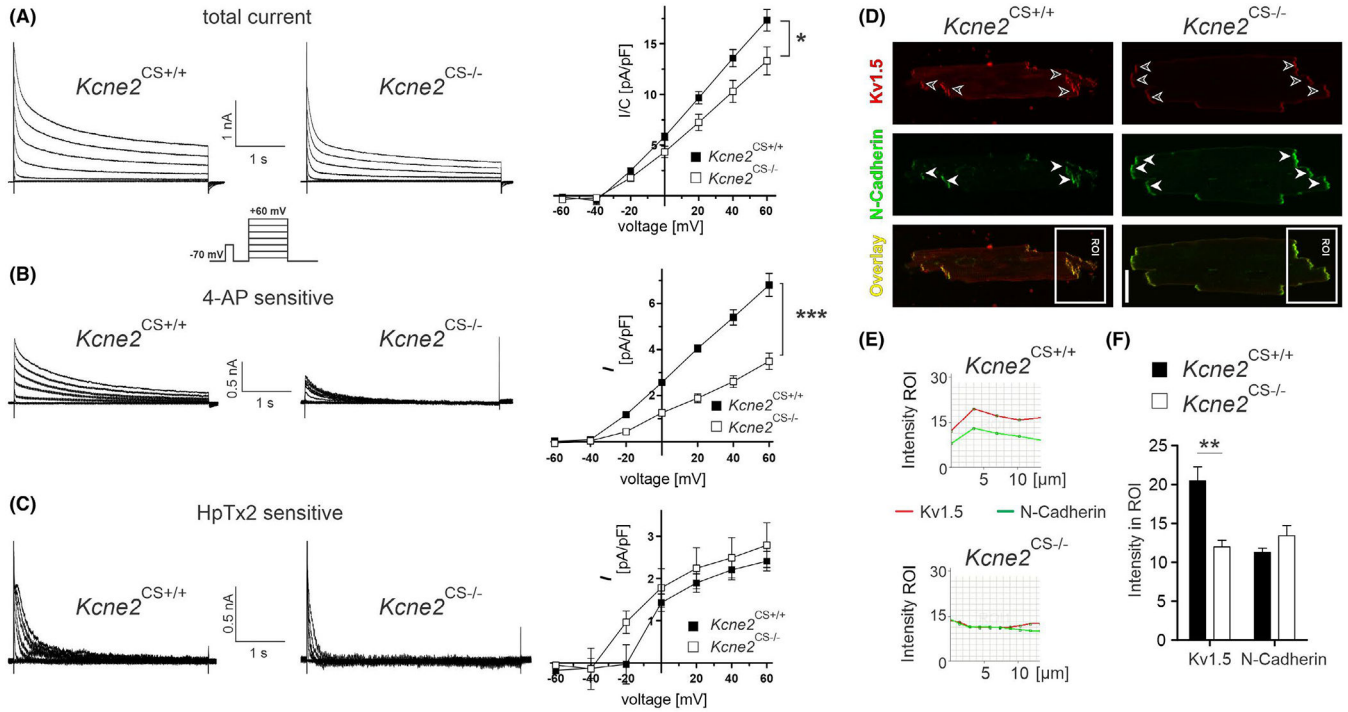

FIGURE 2.

Cardiac-specific *Kcne2* deletion decreases ventricular myocyte Kv current density. A, *Left*: Exemplar whole cell Kv currents recorded from single ventricular cardiomyocytes isolated from $Kcne2^{CS+/+}$ and $Kcne2^{CS-/-}$ mice. *Right*: Mean *I/V* relationship for peak Kv currents recorded in $Kcne2^{CS+/+}$ and $Kcne2^{CS-/-}$ ventricular cardiomyocytes. Peak outward Kv current densities were decreased in cardiomyocytes from $Kcne2^{CS-/-}$ (15 cells, n = 5 mice) compared to $Kcne2^{CS+/+}$ (12 cells, n = 5 mice) mice. $*P < .05$ vs $Kcne2^{CS+/+}$ cells. B and C, Effects of cardiac-specific *Kcne2* deletion on mouse ventricular Kv currents sensitive to 4-AP (panel B; 11–15 cells, n = 5 mice per genotype) and HpTx2 (panel C; 9–10 cells, n = 5 mice per genotype). Kv currents were recorded from $Kcne2^{CS+/+}$ and $Kcne2^{CS-/-}$ myocytes during a 4.5-s depolarizing voltage step to −60 to +60 mV from holding potential of −70 mV (protocol inset). Antagonist-sensitive current traces for each cell were obtained offline by digital subtraction of traces recorded from those recorded before application. *Left*: Exemplar traces of antagonist-sensitive currents recorded from ventricular cardiomyocytes from $Kcne2^{CS+/+}$ and $Kcne2^{CS-/-}$ mice as indicated. *Right*: Mean *I/V* relation for antagonist-sensitive currents recorded in isolated ventricular cardiomyocytes from $Kcne2^{CS+/+}$ and $Kcne2^{CS-/-}$ mice. 4-AP-sensitive currents are significantly reduced in $Kcne2^{CS-/-}$ mice compared to $Kcne2^{CS+/+}$ littermates. In contrast, peak HpTx2-sensitive currents remained unchanged between genotypes (but see further analysis in Results section). Data expressed mean ± SEM. $***P < .001$ vs $Kcne2^{CS+/+}$ cells. D, Double immunostaining with antibodies against Kv1.5 and N-cadherin revealed localization of Kv1.5 (red) and N-Cadherin (green) at the ICD. In $Kcne2^{CS+/+}$ cardiomyocytes Kv1.5 was predominantly detectable within the ICD region. DAPI was used for nucleus staining (blue) Scale bar 25 μm. ROI, regions of interest (containing ICDs). E, Exemplar intensity plots for regions of interest (ROI). F,

Quantitative immunofluorescence analyses of Kv1.5 signals in ROI, 4–6 cells per group). Data expressed mean ± SEM. $^{**}P < .05$ vs matched *Kcne2*$^{CS+/+}$ mice

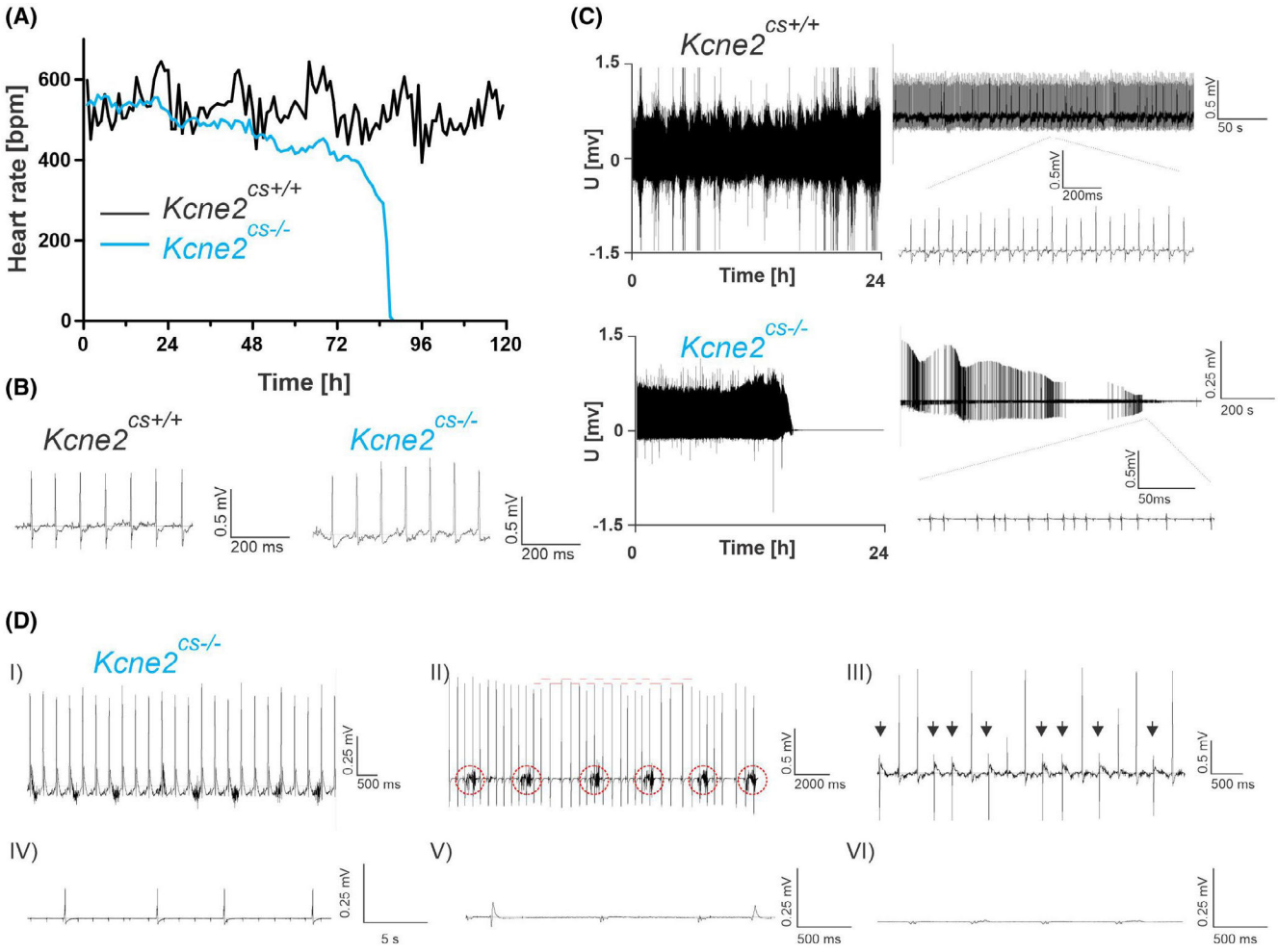

FIGURE 3.

Cardiac-specific *Kcne2* deletion causes progressive bradycardia, AV-Block, and electromechanical dissociation. A, Holter monitor-recorded heart rate over 5 consecutive days for an exemplar conscious $Kcne2^{CS+/+}$ mouse (black) and for the final 3.5 days before death of an exemplar conscious $Kcne2^{CS-/-}$ mouse (blue) at 6 months of age. B, At the beginning of ECG registration both groups display normal sinus rhythm with similar heart frequency. C, Holter monitor-recorded ECG of representative $Kcne2^{CS-/-}$ mouse on the day of death, and for a $Kcne2^{CS+/+}$ mouse over 24 hours. *Right*, ECG recordings in higher magnification. Compared to $Kcne2^{CS+/+}$, $Kcne2^{CS-/-}$ mice display progressive bradycardia over the time period of ECG registration which at first is sinus arrhythmia, with sinus bradycardia followed by progressive AV-block (I°, II°, and finally III°) and finally broad and deformed QRS complexes as a sign of ventricular escape rhythm and electromechanical dissociation. D, ECG pathologies on the day of death in $Kcne2^{CS-/-}$ mice: I) Sinus bradycardia (prolonged RR-interval up 500 ms). II) Sinus arrhythmia with bradycardia (every P-wave is followed by a QRS complex; red line indicates irregular RR-Interval). Red circles indicate artifacts in ECG registration with a frequency of 15 per min represent gasping of the animals as a sign of dyspnea due to severe heart failure. III) Spontaneous ventricular extrasystole indicated by arrows as a sign of enhanced ectopic ventricular

activity. IV) Higher degree AV-block with different AV-conduction. V) Broadened and deformed QRS complexes irregularly appearing during agony phase. VI) Isoelectric line without electrical activity

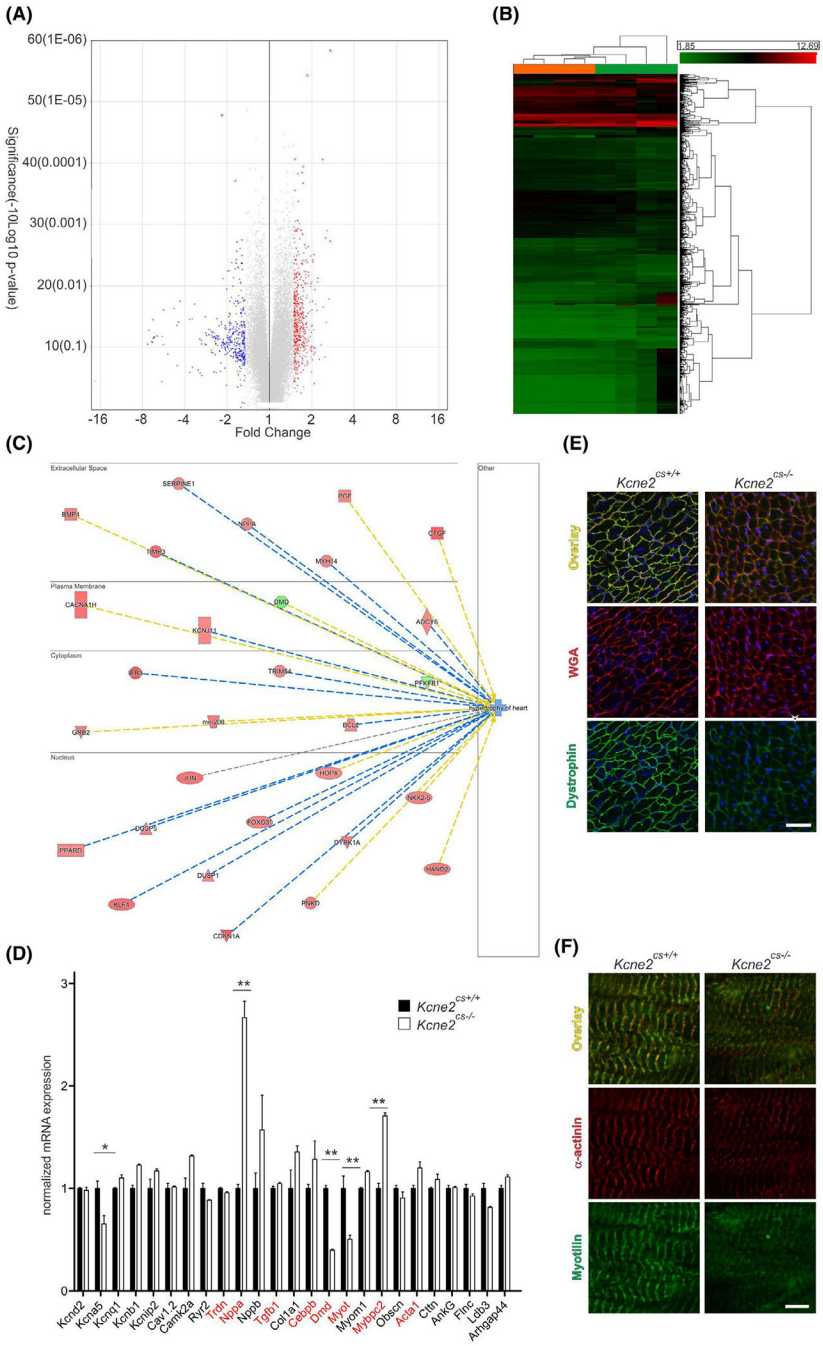

FIGURE 4.

Cardiac-specific *Kcne2* deletion causes DCM-like ventricular remodeling. A, Volcano plot showing DEGs with significant alteration ($P < .05$) in $Kcne2^{CS-/-}$ vs $Kcne2^{CS+/+}$ mouse hearts, generated from the results of microarray transcriptomic analysis (n = 4 mice per genotype). B, Heatmap showing the results of hierarchical analysis of filtered data from microarray analysis. C, Pathway analysis showing DEGs in pathways associated with cardiac hypertrophy, extracted from the results of microarray transcriptomic analysis as in A, using Ingenuity Pathway Analysis. D, Real-time qPCR panel of expression changes for

select genes in *Kcne2*$^{CS-/-}$ ventricle vs *Kcne2*$^{CS+/+}$ controls. Genes suggested by microarray data are shown in red. Data expressed as mean ± SEM, **P* < .05 and ***P* < .01 vs *Kcne2*$^{CS+/+}$ hearts, n = 4–6 mice per genotype). See Table S2 and Supplementary references for full gene names and details. E, Co-immunostaining of dystrophin and wheat germ agglutinin (WGA) to visualize the cell membrane in *Kcne2*$^{CS-/-}$ heart sections compared to wild-type controls. Bar = 50 μm. F, Co-Immunostaining of myotillin and α-actinin in ventricular sarcomeres of *Kcne2*$^{CS-/-}$ vs *Kcne2*$^{CS+/+}$ controls. Bar = 50 μm

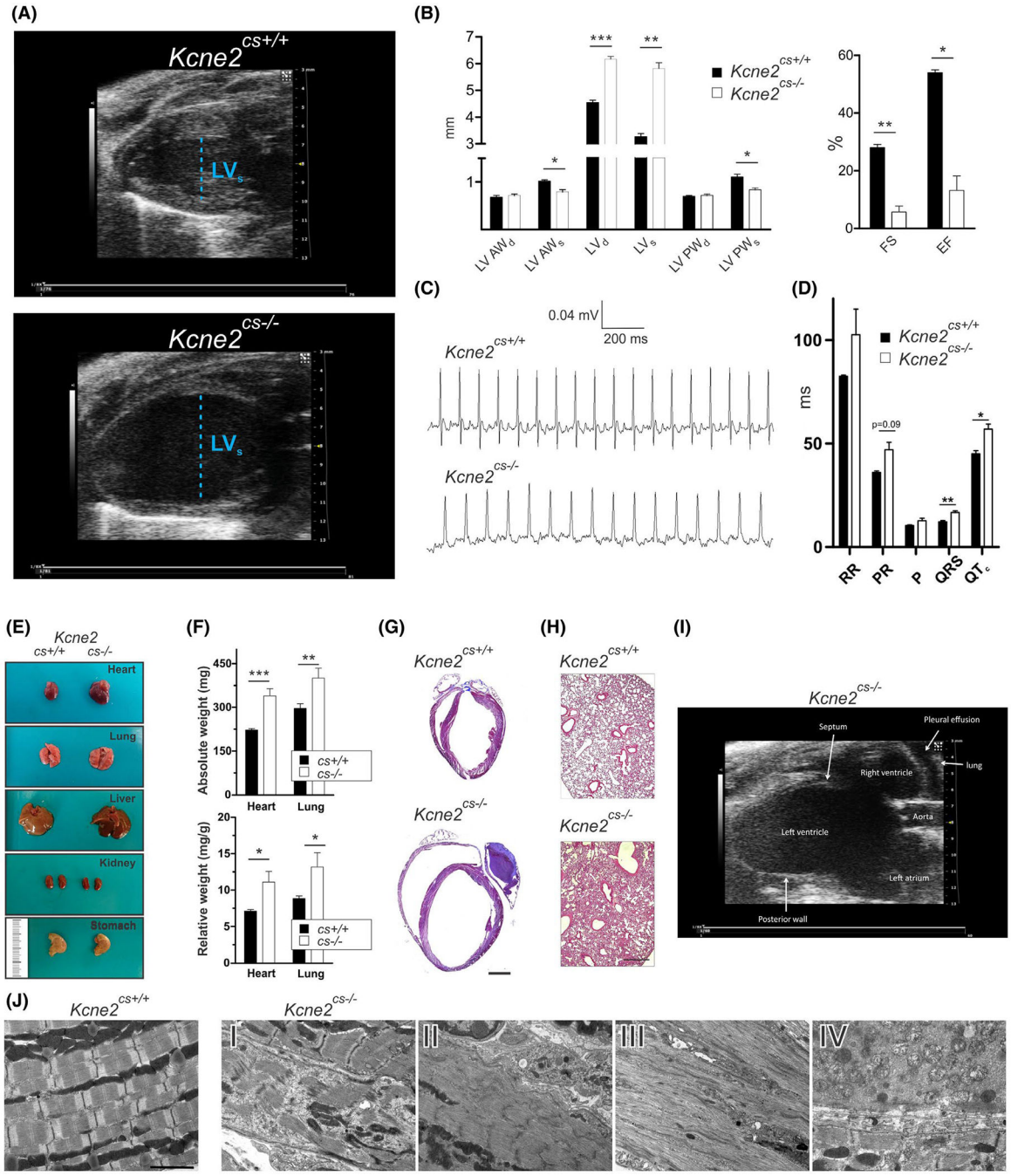

FIGURE 5.

Cardiac-specific *Kcne2* deletion causes early-onset DCM and terminal HF. A, Exemplar 2D parasternal long axis echocardiography traces showing dilation of left ventricle in $Kcne2^{CS-/-}$ mice compared to normal parameters in $Kcne2^{CS+/+}$ mice. B, Mean echocardiographic parameters for mice as in panel A, from M-mode echocardiograms (or 2D parasternal long axis echocardiograms, for ejection fractions). d/s, diastolic/systolic; upper panel, internal diameters: LVAW, left ventricular anterior wall thickness; LVID, left ventricular internal diameter; LVPW, left ventricular posterior wall thickness; lower

panel, functional parameters: EF, ejection fraction; FS, fractional shortening and cardiac output; n = 4 per group. *$P < .05$; **$P < .001$; ***$P < .001$. C, Representative ECG traces from *Kcne2*$^{CS-/-}$ vs *Kcne2*$^{CS+/+}$ mice. D, Mean ECG parameters from traces as in panel c. RR: interbeat interval; PR: PR interval; P: P-wave; QRS: QRS complex; QT_c: corrected QT interval by Bazett's formula; values represent means ± SEM. n = 4 per group. *$P < .05$; **$P < .001$. E, Postmortem gross anatomy of the cardiorespiratory system, liver, kidney, and stomach. *Right*, organs from *Kcne2*$^{CS-/-}$ mice. *Left*, wild-type controls. F, Heart and lung weights for wild-type vs *Kcne2*$^{CS-/-}$ mice in the presence of terminal heart failure. *$P < .05$; **$P < .01$; ***$P < .001$ *Kcne2*$^{CS-/-}$ vs control mice. G, Masson trichrome staining demonstrates fibrosis, dilatation of all chambers, and atrial thrombus in *Kcne2*$^{CS-/-}$ hearts. Bar = 1 mm. H, H&E staining shows lung edema in *Kcne2*$^{CS-/-}$ lung parenchyma. Bar = 500 μm. I, Annotated exemplar M-mode transthoracic echocardiography trace pleural effusion in *Kcne2*$^{CS-/-}$ mice. See associated video files (Videos S1–S3) showing echocardiographic evidence of the severity of HF in *Kcne2*$^{CS-/-}$ mice. J, Ultrastructural features of left ventricle in *Kcne2*$^{CS-/-}$ mice. Left, exemplar ultrastructure of wild-type cardiomyocytes showed normal sarcomere structure. Right site: Ultrastructural analysis of left ventricle biopsies showed different stages of derangement of myofilaments in *Kcne2*$^{CS-/-}$ hearts indicated by focal sarcomere damage (I and II), loss of sarcomere structure (III) and complete loss of sarcomere structure and swollen mitochondria (IV). Bar = 2 μm

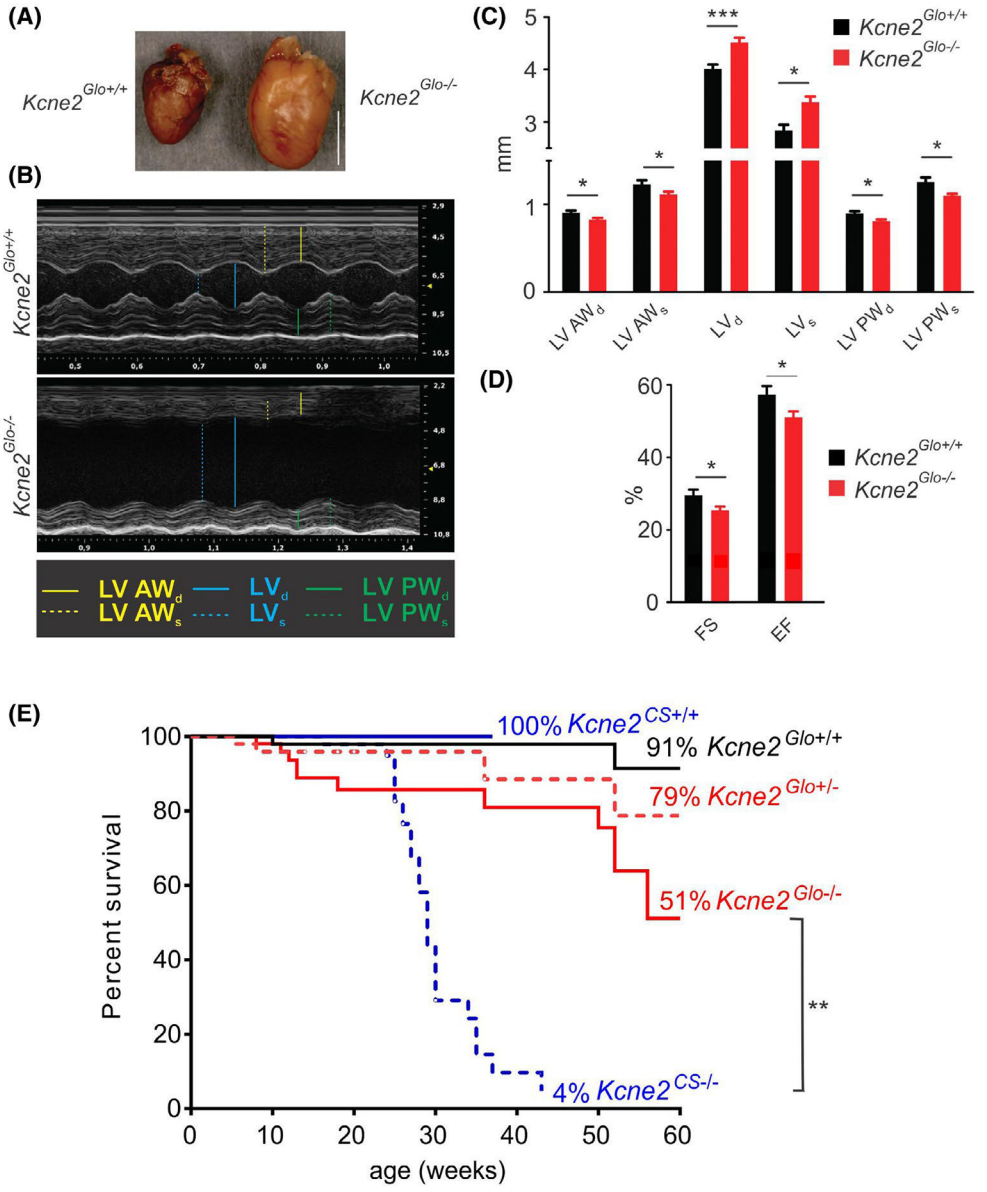

FIGURE 6.

Kcne2$^{Glo-/-}$ mice live longer than *Kcne2*$^{CS-/-}$ mice. A, Macroscopic gross anatomy shows cardiomegaly in 1-y-old *Kcne2*$^{Glo-/-}$ mice. Bar: 5 mm. B, Exemplar echocardiographic M-mode traces showing chamber dilation in aged *Kcne2*$^{Glo-/-}$ mice compared to wild-type littermates. LVAW: anterior left ventricular wall, PW: posterior left ventricular wall, LV: diameter of left ventricle in systole (s) and diastole (d). C, Transthoracic echocardiography reveals DCM with reduced systolic function in aged *Kcne2*$^{Glo-/-}$ mice (12–15 months). Chamber quantification from traces revealed significant LV dilation in 12–15 months old *Kcne2*$^{-/-}$ mice (n = 10 mice per genotype) with a significant increase in left wall thicknesses. *$P < .05$; ***$P < .001$, student's *t* test. D, Global systolic function was impaired in *Kcne2*$^{Glo-/-}$ mice as indicated by mildly reduced left ventricular ejection fraction (EF) and fractional shortening (FS). Values represent means ± SEM. * $P < .05$, student's *t* test. E, Kaplan-Meier survival curves for *Kcne2*$^{Glo+/+}$, *Kcne2*$^{Glo\pm}$, and *Kcne2*$^{Glo-/-}$ mice (n =

50 mice per genotype at time-point zero). Data for untreated $Kcne2^{CS+/+}$ and $Kcne2^{CS-/-}$ (blue curves) from Figure 1 (n = 25–33) shown for comparison. Statistical comparisons were performed for untreated $Kcne2^{CS-/-}$ mice vs omeprazole-treated $Kcne2^{CS-/-}$ mice and untreated $Kcne2^{Glo-/-}$ mice; $^{**}P < .01$, student's *t* test

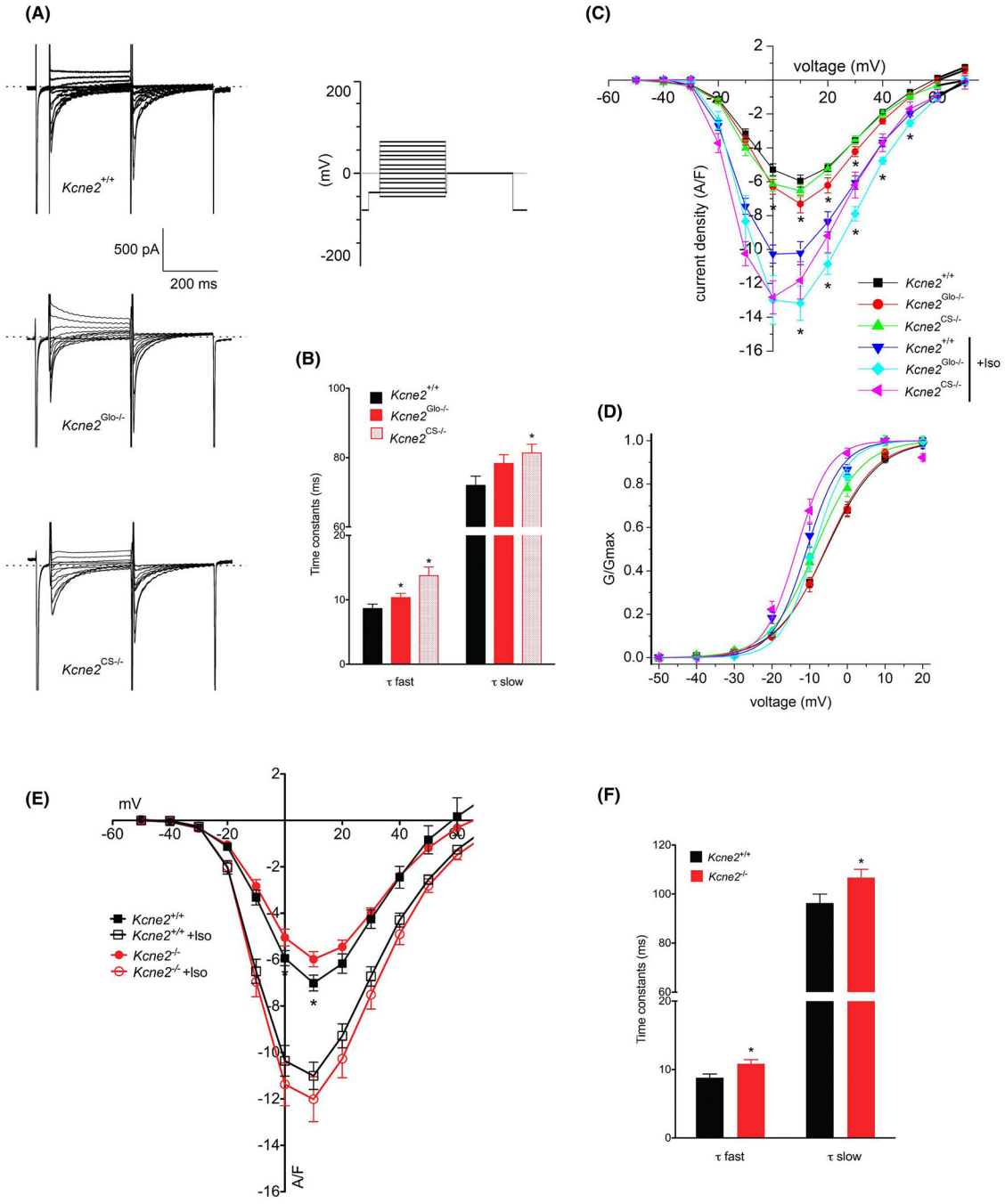

FIGURE 7.

Effects of global vs cardiac-specific Kcne2 knockout on L-type Ca^{2+} current. A, Representative (of n = 9–11 cells per genotype) patch-clamp recordings from isolated ventricular cardiomyocytes freshly isolated from 3 to 6 month-old wild-type, *Kcne2*$^{Glo-/-}$ or *Kcne2*$^{CS-/-}$ mice as indicated, using voltage protocol shown (*upper right*). Dashed line indicates zero current level. B, Comparison of inactivation kinetics for baseline currents shown in panel A; n = 9–11 cells from at least three mice per genotype, **P* < .05 vs wild-type, same treatment group, student's *t* test. Time constants generated by double

exponential fit. C, L-type calcium current densities in isolated ventricular cardiomyocytes from 3 to 6 month-old wild-type, *Kcne2*$^{Glo-/-}$ or *Kcne2*$^{CS-/-}$ mice as indicated, at baseline or following isoproterenol treatment (+Iso); n = 9–11 cells from at least three mice per genotype, *$P < .05$ vs wild-type, same treatment group, student's *t* test. D, Normalized G/Gmax plot for currents as in panel C. E, L-type calcium current densities in isolated ventricular cardiomyocytes from 12 to 15-month-old wild-type and *Kcne2*$^{Glo-/-}$ mice as indicated, at baseline or following isoproterenol treatment (+Iso); n = 16–17 cells of at least three mice per genotype, *$P < .05$ vs wild-type, same treatment group, student's *t* test. F, Comparison of inactivation kinetics for baseline currents shown in panel C; n = 16–17 cells from at least three mice per genotype, *$P < .05$ vs wild-type, same treatment group, student's *t* test. Time constants generated by double exponential fit

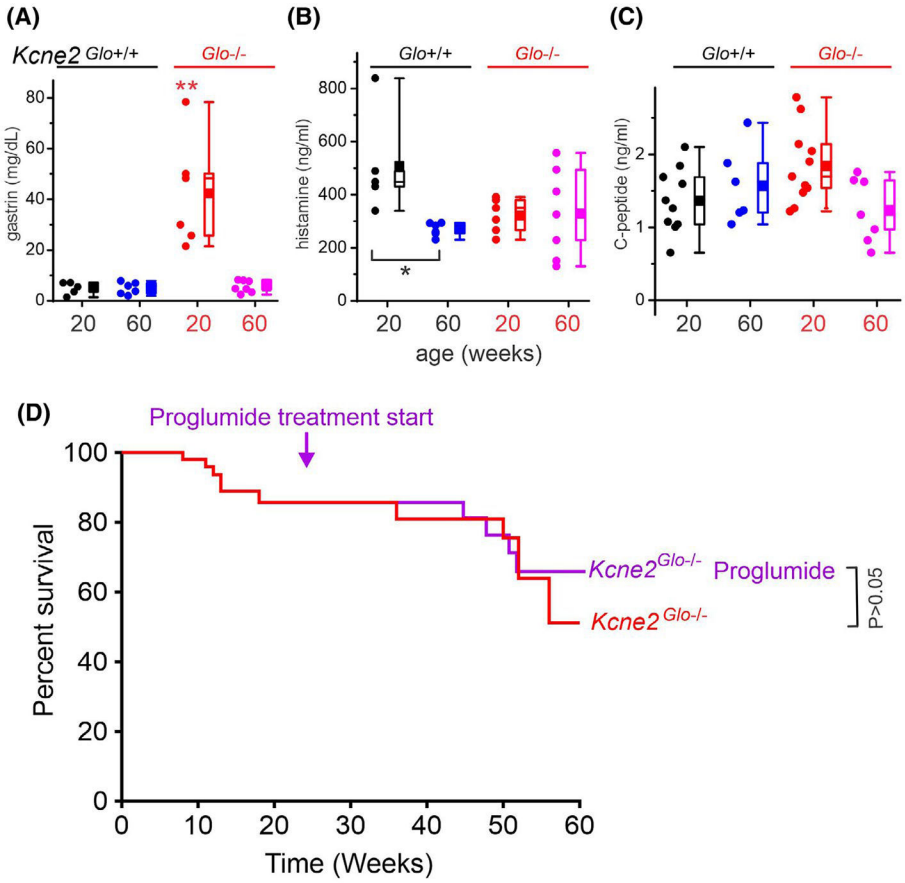

FIGURE 8.

Gastrin receptor inhibition does not alter survival of *Kcne2*$^{Glo-/-}$ mice. A-C, Serum concentrations of gastrin (a), histamine (b), and C-peptide (c) in 20- vs 60- week-old male *Kcne2*$^{Glo+/+}$ and *Kcne2*$^{Glo-/-}$ mice (n = 5–11). *P < .05; **P < .01 vs all other groups; both after Bonferroni correction; all other comparisons P > .05 after Bonferroni correction. D, Kaplan-Meier survival curves for untreated *Kcne2*$^{Glo-/-}$ mice (n = 50 mice per genotype at time-point zero), compared to proglumide-treated *Kcne2*$^{Glo-/-}$ mice (n = 19 mice at time-point zero); P > .05

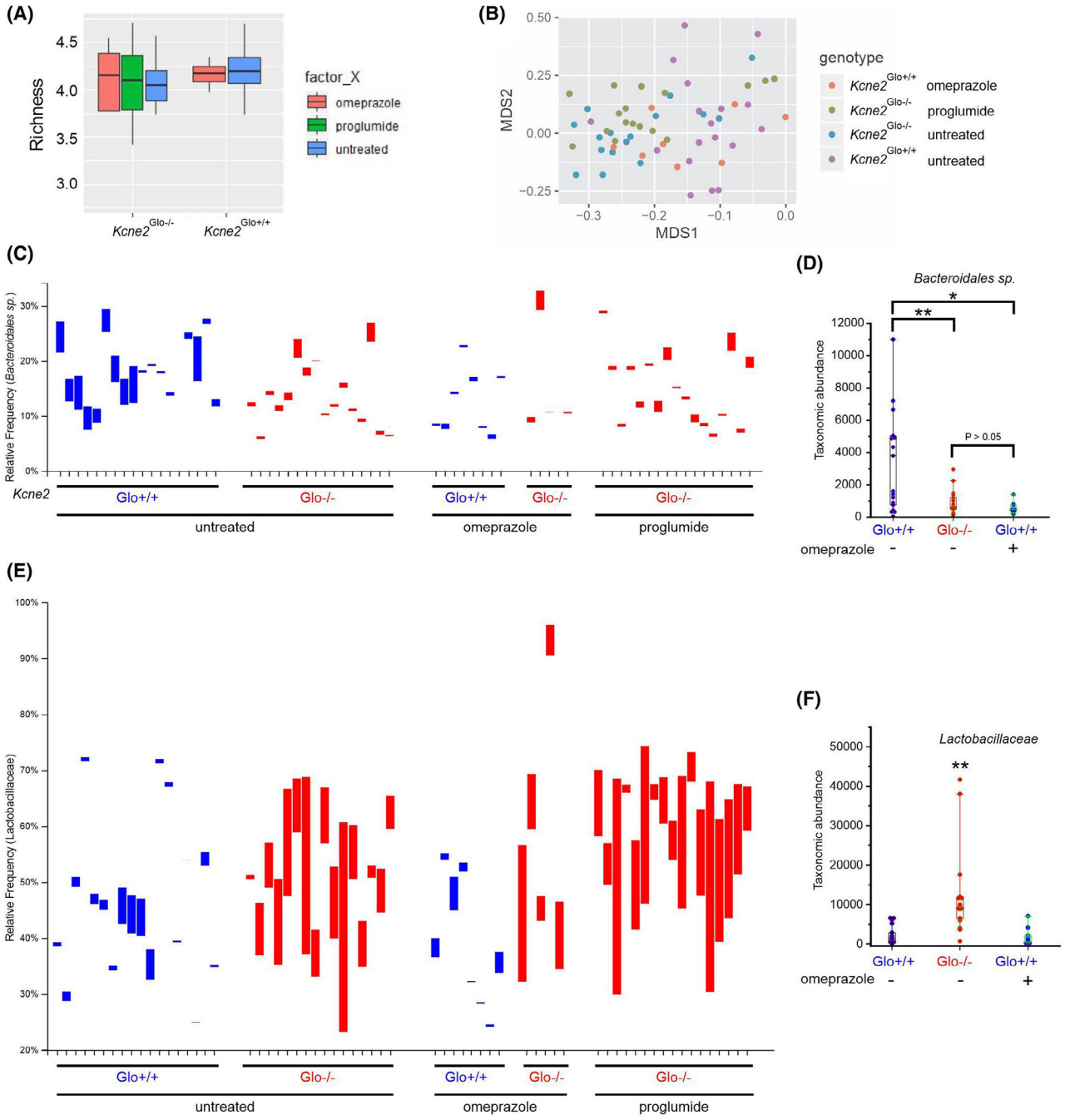

FIGURE 9.

Omeprazole treatment and global *Kcne2* knockout similarly decrease relative abundance of a subset of *Bacteroidales* in the gut. A, Shannon alpha diversity of the gut microbiomes in the genotypes and treatment groups indicated (n = 5–18). B, Principal Coordinates Analysis (PCoA) plot of dissimilarity (beta diversity) of the gut microbiomes in the genotypes and treatment groups indicated (n = 8–18). C, Relative frequency in the genotypes and treatment groups shown of the Bacteroidales group "g-, f-," subset (n = 5–18). Each bar represents the gut microbiome of one mouse; the size of each bar on the y axis scale represents

the relative frequency of Bacteroidales species. D, Box plots showing statistical analysis of data in panel c. Error bars indicate SEM; n = 5–18. *$P < .05$; **$P < .01$. E, Relative frequency in the genotypes and treatment groups shown of the Lactobacillaceae (n = 5–18). Each bar represents the gut microbiome of one mouse; the size of each bar on the y axis scale represents the relative frequency of Lactobacillaceae. F, Box plots showing statistical analysis of data in panel E. Error bars indicate SEM; n = 5–18. **$P < .01$ vs other groups

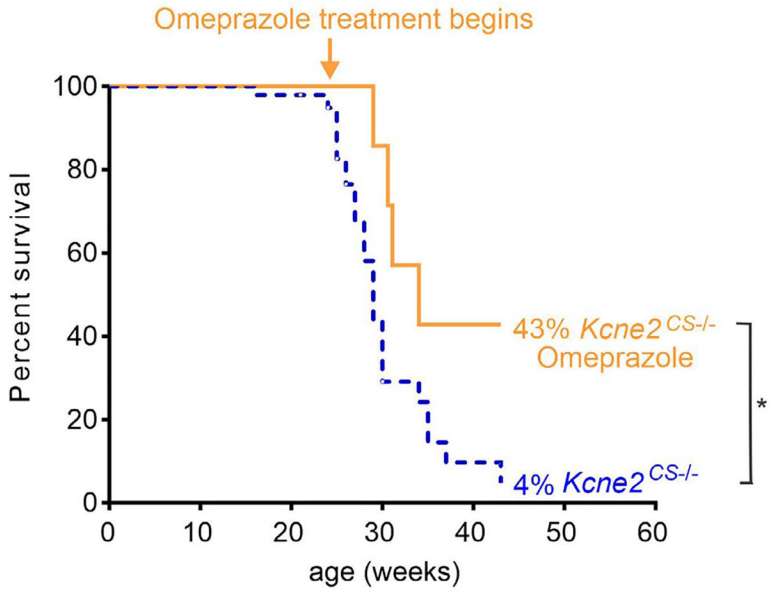

FIGURE 10.

Omeprazole delays terminal HF in *Kcne2*$^{CS-/-}$ mice. Kaplan-Meier survival curves for untreated *Kcne2*$^{CS-/-}$ mice (n = 25; from Figure 1) and omeprazole-treated *Kcne2*$^{CS-/-}$ mice (n = 7); **P* < .05